UNIVERSITY OF CALIFORNIA, SAN DIEGO

Lab-on-a-chip flow cytometer and microfluidic fluorescence activated cell sorter (μFACS) for biomedical applications

A dissertation submitted in partial satisfaction of

the requirements for the degree Doctor of Philosophy

in

Materials Science and Engineering

by

Sung Hwan Cho

Committee in charge:

Professor Yu-Hwa Lo, Chair
Professor Prabhakar Bandaru
Professor Jennifer Cha
Professor Sungho Jin
Professor Kun Zhang

2010

The dissertation of Sung Hwan Cho is approved, and it is acceptable in quality and form for publication on microfilm and electronically:

_____

_____

_____

_____

_____

Chair

University of California, San Diego

2010

Dedication

This dissertation is dedicated to my parents.

Table of Contents

List of Figures

List of Tables

Acknowledgements

At the outset, I would like to express my sincere gratitude to my adviser Prof. Yu-Hwa Lo for his enormous support and consistent faith in me. I would like to thank him for continual encouragement over the course of my last four years of research in his group. My original background, Materials Science and Engineering, was quite different from his research fields, which made working within his group a very challenging experience, at first. However, he believed in me and helped me to make my research experience during the course of my Ph.D exciting, inspiring, and very interesting. As a result, it allowed me to make several key contributions to the new research fields – biophotonics and lab-on-a-chip microfluidic devices for biomedical applications. Research-wise, he has helped me identify the difference between fundamental scientific research and engineering. He always emphasized the importance of hard work and persistency as an independent researcher in order to have deep insights. He did not give direct answers, but rather asked me to see the problem I was facing from a different perspective, enhancing my creativity. Even though my Ph.D thesis was about developing lab-on-a-chip flow cytometer devices, he always encouraged me to be actively involved in other interesting research projects such as the SurgiCam project or intraocular lens project using bio-inspired fluidic lenses. I attended those project meetings and finally contributed to the projects by fabricating devices or building up measurement optical imaging systems with co-workers. While working on many multidisciplinary projects, I met a variety of people with different backgrounds and learned how to collaborate with them as a team in an efficient way. I am very grateful

to have him as my advisor during my PhD studies as he has helped me tremendously in my growth during one of the most crucial moments of my life.

I also thank the other members of the dissertation committee, Prof. Sungho Jin, Prof. Prabhakar Bandaru, Prof. Kun Zhang, and Prof. Jennifer Cha. They contributed, not only to the direction of this work, but also to my development as a scientist and engineer. In particular, I would like to express my deep appreciation to Prof. Sungho Jin and Prof. Bandaru for supporting me financially in my first year.

The project performed in my research is interdisciplinary, and it is a difficult task to be accomplished by one person alone. Many of the achievements are collective contributions from several people, and I would like to acknowledge them for their efforts to collaborate with me to get things done. All of the lab mates and colleagues I have learned from and worked with at UCSD are people I am indebted to, who deserve much appreciation. I would like to express my gratitude to my lab mates who have been working with me on several interesting projects: Jessica Godin was the research mentor of mine in my first year of the group and she was a great role model in performing independent research as a graduate student. Chun-Hao (Randy) Chen has collaborated with me on the μFACS project, and we have been very productive throughout them. Frank S. Tsai is the person who I spent most of my time together in the lab, and I learned many things from him, including optics, signal processing, all the simulation tools, and so on. Wen Qiao has been involved in many of my research work, and we coauthored several publications out of the productive discussion and collaboration. I also would like to thank Kai Zhao, Arthur Zhang, Ashkan Arianpour, Shawn Meade,

Vyacheslav Gomon, Hosuk Lee, Tsung-Fong Wu and Kenichi Yamashita for their contribution and suggestions.

I also would like to thank Sam Chiang and Jeff Gole in Prof. Kun Zhang's group for helping me sort bacteria samples for the human microbiome project, as it has helped explore a very exciting research field using our own technologies.

The well being of nano3 clean room facilities and the fabrication of most of the devices for my study would not have been possible without the hard work and dedication of Dr. Bernd Fruhberger, Dr. Maribel Montero, Dr. Xuekun Lu, Larry Grissom, Ryan Anderson and Sean Parks. I am very thankful for their assistance.

My lovely wife Eun Young, and my adorable children Hyoungho and Emily kept me motivated and enabled me to sustain all the challenges I have met in the course of my Ph.D. program. From time to time, it seemed very challenging or nearly impossible to keep a good balance between my work and family life, thus leading to lots of stress and strains on the relationships with my family members. However, we have successfully overcome all the sufferings and challenges together as a family, and we are about to move on to our new life soon. It goes without saying that I could not have done much of anything without their support, sacrifice and love.

Last but not the least; I owe all of my achievements to my parents for their profound love, patience, sacrifice, trust and encouragement throughout my entire life. As your son, it is with boundless joy and gratitude that I now dedicate this thesis to you.

Chapter 1 or portion thereof has been published in *Lab on a Chip* 2010, S. H. Cho, C.-H. Chen, J. M. Godin, F. S. Tsai, and Y.-H. Lo. The dissertation author was the first author of the paper.

Chapter 3 or portion thereof has been published in *IEEE Photonics Technology Letters* 2009, S. H. Cho, J. M. Godin, and Y.-H. Lo. The dissertation author was the first author of the paper.

Chapter 4 or portion thereof has been published in *Lab on a Chip* 2010, S. H. Cho, C.-H. Chen, J. M. Godin, F. S. Tsai, and Y.-H. Lo. The dissertation author was the first author of the paper.

Chapter 5 or portion thereof has been published in *Applied Physics Letters* 2010, S. H. Cho, W. Qiao, F. S. Tsai, K. Yamashita, and Y.-H. Lo. The dissertation author was the first author of the paper.

Appendix or portion thereof has been published in *Optics Letters* 2009, S. H. Cho, F. S. Tsai, W. Qiao, N.-H. Kim, and Y.-H. Lo. The dissertation author was the first author of the paper

Vita

February, 2004	Bachelor of Science in Materials Science and Engineering Seoul National University, Seoul, Korea
2005 – 2010	Graduate Student Researcher Materials Science and Engineering Program Department of Electrical and Computer Engineering University of California, San Diego
December, 2006	Master of Science in Materials Science and Engineering Materials Science and Engineering Program University of California, San Diego
December, 2010	Doctor of Philosophy in Materials Science and Engineering Materials Science and Engineering Program University of California, San Diego

Journal Publications

1. **Sung Hwan Cho**, Jessica M. Godin, Chun-Hao Chen, Wen Qiao, Hosuk Lee, and Yu-Hwa Lo, "Recent advancement in optofluidic flow cytometry," ***Biomicrofluidics*** (2010) – submitted for publication

2. Chun-Hao Chen*, **Sung Hwan Cho***, Sam Chiang, Frank S. Tsai, Kun Zhang, and Yu-Hwa Lo, "An integrated μFACS technology combined with Tyramide Signal Amplification enhanced Fluorescence in situ Hybridization for isolation of rare bacteria and removal of cell-free DNA", *: Equally contributed, manuscript in preparation

3. Chun-Hao Chen, **Sung Hwan Cho**, Nicole Justice, and Yu-Hwa Lo, "A nozzle/diffuser-based cell sorter using piezoelectric actuation," submitted to ***Microfluidics and Nanofluidics*** (2010)

4. **Sung Hwan Cho**, Wen Qiao, Frank S. Tsai, Kenichi Yamashita, and Yu-Hwa Lo, "Lab-on-a-chip flow cytometry employing color-space-time coding," ***Applied Physics Letters***, 96, 1 (2010)

5. **Sung Hwan Cho***, Chun-Hao Chen*, Frank S. Tsai, Jessica M. Godin, and Yu-Hwa Lo, "Human mammalian cell sorting using microfabricated fluorescence activated cell

sorter," ***Lab on a Chip***, **10**, 1567 (2010) *: Equally contributed

6. Frank S. Tsai, Daniel Johnson, Cameron Francis, **Sung Hwan Cho**, Wen Qiao, Ashkan Arianpour, Yoav Mintz, Santiago Horgan, Mark Talamini, and Yu-Hwa Lo, "Fluidic lens laparoscopic zoom camera for minimally invasive surgery," ***Journal of Biomedical Optics***, 15 (3), May/June (2010)

7. Chun-Hao Chen, **Sung Hwan Cho**, Frank S. Tsai, Ahmet Erten, and Yu-Hwa Lo, "Microfluidic cell sorter with integrated piezoelectric actuator," ***Biomedical Microdevices***, 1572 (2009)

8. Wen Qiao, Daniel Johnson, Frank S. Tsai, **Sung Hwan Cho**, and Yu-Hwa Lo, "Bio-Inspired Accommodating Fluidic Intraocular Lens," ***Optics Letters***, **34,** 20 (2009), also published in ***Virtual Journal for Biomedical Optics*** (2009)

9. **Sung Hwan Cho**, Jessica M. Godin, and Yu-Hwa Lo, "Optofluidic waveguides in Teflon-coated microfluidic channels," ***IEEE Photonics Technology Letters***, **21**, 15 (2009), also published in ***Virtual Journal of Laser*** (2009)

10. Wen Qiao, Frank S. Tsai, **Sung Hwan Cho**, Huimin Yan, and Yu-Hwa Lo, "Fluidic intraocular lens with a large accommodation range," ***IEEE Photonics Technology Letters***, **21**, 5, 304 (2009)

11. **Sung Hwan Cho**, Frank S. Tsai, Wen Qiao, Nam-Hyong Kim, and Yu-Hwa Lo, "Fabrication of Aspherical Polymer Lenses Using Tunable Liquid-Filled Mold," ***Optics Letters***, **34**, 5, 605 (2009)

12. Jessica Godin, Chun-Hao Chen, **Sung Hwan Cho**, Wen Qiao, Frank S. Tsai, Yu-Hwa Lo, "Microfluidics and photonics for Bio-System-on-a-Chip: A review of advancements in technology towards a microfluidic flow cytometry chip" ***Journal of Biophotonics***, **1**, 5, 355 (2008)

13. Frank S. Tsai, **Sung Hwan Cho**, Yu-Hwa Lo, Bob Vasko, and Jeff Vasko, "Miniaturized Universal Imaging Device Using Fluidic Lens," ***Optics Letters***, **33**, 3, 291 (2008), also published in ***Virtual Journal for Biomedical Optics*** (2009)

Conference Proceedings

1. Frank S. Tsai, Daniel Johnson, **Sung Hwan Cho**, Wen Qiao, Ashkan Arianpour, Cameron Francis, Nam-Hyong Kim, and Yu-Hwa Lo, "Integrated bio-inspired fluidic imaging system," ***SPIE Photonics West***, San Francisco, CA, Jan (2010), **(Invited)**

2. **Sung Hwan Cho**, Chun-Hao Chen, Frank S. Tsai, Jessica M. Godin, Yu-Hwa Lo, "Human mammalian cell sorting using μFACS," ***CLEO/QELS***, San Jose, CA, May (2010)

3. Frank S. Tsai, Daniel Johnson, Cameron Francis, **Sung Hwan Cho**, Wen Qiao, Ashkan Arianpour, and Yu-Hwa Lo, "Fluidic lens laparoscopic zoom camera for minimally invasive surgery," ***CLEO/QELS***, San Jose, CA, May (2010)

4. Jessica M. Godin, **Sung Hwan Cho**, and Yu-Hwa Lo, "On-chip optics for manipulating light in polymer chips," ***OptoElectronics and Communications Conference (OECC) 14th***, Shanghai, China (2009) **(Invited)**

5. Frank S. Tsai, Daniel Johnson, **Sung Hwan Cho**, Wen Qiao, Ashkan Arianpour, and Yu-Hwa Lo, "Bio-inspired fluidic lens enhanced surgical camera for MIS," ***IEEE EMBC***, Minneapolils, MN, Sep. (2009)

6. Wen Qiao, Daniel Johnson, Frank S. Tsai, **Sung Hwan Cho**, and Yu-Hwa Lo, "An Accommodating Fluidic Intraocular Lens Design and Process," ***IEEE EMBC***, Minneapolils, MN, Sep. (2009)

7. **Sung Hwan Cho**, Chun H. Chen, Frank S. Tsai, and Yu-Hwa Lo, "Automated Real-time sorting with high throughput microfabricated fluorescence-activated cell sorter," ***IEEE EMBC***, Minneapolils, MN, Sep. (2009)

8. **Sung Hwan Cho**, Jessica Godin, Chun Hao Chen, Frank S. Tsai, Yu-Hwa Lo, "Microfluidic Photonic Integrated Circuits," ***SPIE APOC***, Oct. (2008) **(Invited)**

9. Wen Qiao, Frank S. Tsai, **Sung Hwan Cho**, Huimin Yan, Yu-Hwa Lo, "Tunable Fluidic Intraocular Lens in Human Eye Model," ***OSA Frontiers in Optics*****,** OSA Technical Digest (CD), Optical Society of America, (2008)

10. **Sung Hwan Cho**, Frank S. Tsai, Wen Qiao, Nam-Hyong Kim, and Yu-Hwa Lo, "Fabrication of Polymer Lenses Using Liquid-Filled Mold," ***Proceedings in UKC 2008***, San Diego, CA, USA, Aug. (2008)

11. Frank S. Tsai, **Sung Hwan Cho**, Wen Qiao, Nam-Hyong Kim, and Yu-Hwa Lo, "Miniaturized Universal Imaging Device Using Bio-inspired Fluidic Lens," ***SPIE O+P***, San Diego, Aug. (2008) **(Invited)**

12. Chun-Hao Chen, **Sung Hwan Cho**, Ahmet Erten, and Yu-Hwa Lo, "High-throughput cell sorter with piezoelectric actuation," ***MicroTAS***, San Diego, CA, Oct (2008)

13. **Sung Hwan Cho**, Frank S. Tsai, Bob Vasko, Jeff Vasko, and Yu-Hwa Lo, "Fluid-Filled Tunable Mold for Polymer Lenses," ***CLEO/QELS***, San Jose, CA, USA, May (2008)

14. Frank S. Tsai, **Sung Hwan Cho**, Yu-Hwa Lo, Bob Vasko, and Jeff Vasko, "Miniature Unified Imaging Device Using Fluidic Lenses," ***IEEE LEOS***, Lake Buena Vista, FL, Oct. (2007)

Book Chapters

1. S. O. Meade, J. Godin, C. H. Chen, **S. H. Cho**, F. S. Tsai, W. Qiao, and Y.-H. Lo, "Microfluidic flow cytometry: Advancement toward compact, integrated systems," in *Advanced optical cytometry: methods and disease diagnoses*; Ed. V. Tuchin, Wiley-VCH, in press (2010)

2. C. H. Chen, J. Godin, **S. H. Cho**, F. S. Tsai, W. Qiao, and Y.-H. Lo, "Flow cytometry and fluorescence-activated cell sorting," in *Handbook of Optofluidics*: Ed. A. Hawkins and H. Schmidt, CRC press (2010)

3. F. S. Tsai, J. Godin, **S. H. Cho**, W. Qiao, and Y.-H. Lo, "Bio-Inspired fluidic lenses for imaging and integrated optics," Chapter 9, in *Optofluidics: Fundamentals, Devices, and Applications*; Ed. Y. Fainman, L. P. Lee, D. Psaltis, C. Yang, McGraw-Hill (2009)

ABSTRACT OF THE DISSERTATION

Lab-on-a-chip flow cytometer and microfluidic fluorescence-activated cell sorter (μFACS) for biomedical applications

by

Sung Hwan Cho

Doctor of Philosophy in Materials Science and Engineering

University of California, San Diego, 2010

Professor Yu-Hwa Lo, Chair

This dissertation details the development of a portable, low cost lab-on-a-chip flow cytometer and/or fluorescence-activated cell sorter (μFACS), in which microfluidics, micro-acoustics, on-chip optics and electronics are integrated into one tiny polydimethylsiloxane (PDMS) chip creating novel functionalities. This work demonstrates a compact, high-speed sorter, integrated optofluidic waveguides, and a novel color-space-time coding technique for low-cost fluorescence detection.

The microfluidic fluorescence-activated cell sorter employs fast-response piezoelectric actuators in conjunction with a high-speed, low timing jitter closed loop control system ensures high purity sorting of targeted biological samples with single-cell

manipulation capabilities. By deflecting the entire sub-nanoliter volume of fluid, the μFACS can sort various biological samples regardless of their physical or chemical properties. A high enrichment factor (>230 fold) is demonstrated at a sorting throughput of greater than 1,000 cells/sec. By integrating the entire sorting system onto the chip, this technology holds great promise to rapidly become competitive with commercial benchtop sorters.

Teflon AF coated optofluidic waveguides demonstrated in this work enhance the coupling efficiency of photons to fluorescent samples, thus increasing sensitivity and permitting multi-spot illumination. The waveguides also enable the space-time coding technology, which works in conjunction with a specially designed spatial filter and the finite-impulse-response (FIR) match filter algorithm in order to further enhance detection sensitivity.

The multi-color fluorescence detection technology with an on-chip color filter waveguide array, known as Color-Space-Time (COST) coding, enables the discrimination of up to 11 fluorescent wavelengths using a single photodetector. This novel technology holds great promise for compactness by fundamentally altering the scaling rule; that is the number of bulky optical components required for detection will no longer scale linearly with the number of detection parameters. In this way, the technique can significantly lower the cost and the volume of the whole system in addition to miniaturization of the device.

Such a low-cost, compact, portable flow cytometer and μFACS system can be readily afforded by individual clinics and research labs, providing point-of-care

diagnosis and analysis. The development of the microfluidic flow cytometer/μFACS can improve global quality of life; and while the technology is not fully ready today, great strides have been made towards achieving this goal, as demonstrated in this dissertation.

Chapter 1

Introduction and Background – Lab-on-a-chip microfluidic flow cytometer and fluorescence-activated cell sorter

There have been increasing needs to develop lab-on-a-chip microfluidic flow cytometers for the past decades. The development of a low-cost, compact and handheld flow cytometer or microfluidic cell sorting system could bring significant impact on to biomedical research or clinical applications such as point-of-care diagnosis. Such

portable yet reliable device platforms could also improve the quality of health care in some underserved areas in Africa or Asia, where people are struggling with epidemics such as HIV/AIDS or malaria etc

In this introduction chapter, the principle of commercial benchtop flow cytometers and fluorescence-activated cell sorters (FACS) will be mentioned fat first, followed by the introduction of their various biological and clinical. The brief survey on the advancements in developing lab-on-a-chip flow cytometers/FACS with advantages and disadvantages of such miniaturized systems are also included later.

1. 1. Flow cytometry – its principle and applications in biomedical research

The flow cytometer, or fluorescence-activated cell sorter (FACS), is an indispensible bio-analysis tool that is widely used in fundamental biomedical research and clinical diagnostics. The flow cytometer gives useful information on both physical and biochemical properties of interested biological samples such as cells, bacteria etc, in a non-destructive and highly quantitative manner at a high screening throughput [1, 2]. Therefore, the flow cytometry is commonly used in various biomedical research fields, such as immunology, cell biology and molecular biology, cell cycle analysis, intracellular cytokine measurement, vaccine analysis, phagocytosis and many more to name a few [3-6]. A state-of-the-art flow cytometer can screen about million cells per second and then sort out a specific, pure subpopulation out of heterogeneous mixtures for further biochemical analysis and genomic studies, thus enabling studies of rare-events such as the isolation of stem cells or circulating tumor cells or many more [7].

Besides its applications in basic biomedical research, flow cytometry has also evolved to become an important clinical tool to allow physicians to monitor the progression of disease such as leukemia and HIV/AIDS [2, 8, 9].

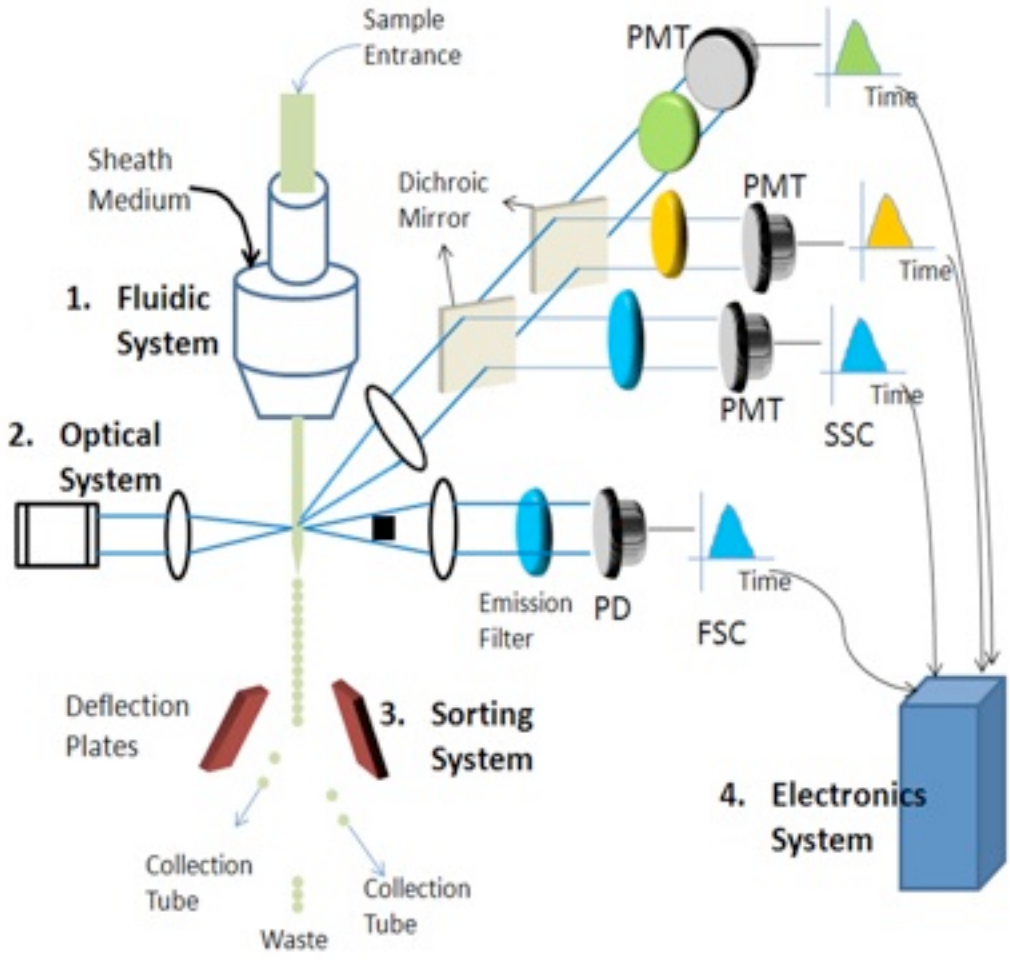

Figure 1. 1 A simplified schematic diagram of typical benchtop fluorescence-activated cell sorter system showing four detection parameters (forward scattering, side scattering, and two fluorescent colors) in conjunction with the sorting system and the electronic control system for data acquisition and determination of sorting events.

Traditional flow cytometry detects scattered and fluorescent light signals out of cells of interest and analyzes the signals in a highly quantitative manner to identify individual cells. A flow cytometer in general consists of four main components as shown in Figure 1.1 above; (1) fluidic system for introducing cells into the system one by one, (2) optical system (both for illumination/excitation and for detection of light signals), (3) electronic control system for acquiring data and for making a decision for sorting cells of interest (4) sorting system for purifying sub-population.

The suspended cells are introduced into the fluidic channel and hydrodynamically focused by sheath flow, ensuring that the cells travel in the center of the fluidic channel at a uniform velocity. Upon arrival at the optical investigation zone, the cells are optically interrogated one by one, by a narrowly focused laser beam (typically 20 μm width) passing vertically across the fluidic channel. Forward scatter collection (FSC), side scatter collection (SSC) and several fluorescence collections (FL) are obtained from each cell simultaneously by the optical detection system consisting of off chip high numerical aperture lenses, dichroic mirrors, filters, and photodetectors such as photomultiplier tubes (PMT).

The forward scattering collection line (covering about 1 ~ 10 degree of scattered light from the laser illumination axis) should see an increase in intensity as cells pass through the focused laser beam. The forward scattering collection generally requires the use of a beam stop to prevent collection of the excessive illumination source in addition to the desired forward light scatter signal. The relative intensity yields information related to size and refractive index of the cells or particles. Similarly, the relative light

intensity collected by the side scattering collection line (typically located at about 90 degree from the laser illumination axis) unveils the degree of internal structure of the cell such as granularity.

In addition to the scattering collection lines, several fluorescent emission lines from fluorescently labeled cells are also collected at the same time. A simple flow cytometer includes about four fluorescent detection channels with two excitation sources; 488 nm and 633 nm. Some of high-end flow cytometers for polychromatic flow cytometry applications can discriminate up to seventeen colors or even more in addition to the forward and side scattering lines [10, 11].

The quality of both the optical and fluidic systems is critical for device performance and reliability. The suspended cells must pass through a small and uniform illumination beam spot at a repeatable location in order to prevent any fluctuation in signal intensities. Both of the scattering and the fluorescent signals must be registered from a single cell only at a time, in other words, no incident events out of two or more cells should be prevented. The signal acquisition process must be free from excess noise such as stray light from the environment, random scattering from debris, uneven channel wall etc.

Photodetectors such as photomultiplier tubes (PMT) register the scattered and fluorescent signals. For fluorescent signals, dichroic mirrors split the emission spectrum to route the desired emission bands to the appropriate PMTs dedicated to the specific wavelength regime, and optical filters further define the wavelength band passed to each PMT more specifically. The registered signal intensities for each parameter are

analyzed to discriminate between various sample subpopulations (e.g. scatter to distinguish monocytes, lymphocytes, and granulocytes in a leukocyte sample, and fluorescence to further distinguish cells by surface antigens, such as CD4+ or CD8+ lymphocytes) [2, 7, 12, 13].

After identification of the cells of interest by the optical system, a downstream sorting system isolates the targeted sample cells according to the information obtained at the upstream detection zone. Precise sorting is typically performed through a droplet-formation approach. As cells of interest approach the sorting junction, the main sample fluid stream is broken into individual electrically charged droplets by vibration, thus allowing their paths to be manipulated by a pair of electrically charged deflection plates. Through a feedback control system (e.g. the decision making process after the cell is detected and identified), the polarity of the electric plates changes in order to deflect the droplets containing cells of interest into the proper collection tubes for further analysis and studies.

1. 2. Microfluidic flow cytometry and micro-FACS (μFACS)

There are many compelling reasons to develop a lab-on-a-chip flow cytometer, preferably with cell sorting capability (i.e. microfluidic FACS systems). Today, FACS systems are typically located in centralized facilities and shared by many researchers due to their high cost, bulky size, and significant cost for maintenance. Unfortunately, such centralized facilities impose huge limits on the accessibility of the powerful and indispensible bioanalysis equipment. In addition, the sorting systems are droplet-based

as explained earlier, and droplets including cells are exposed to air, increasing the possibility of generating bio-hazardous aerosols.

Moreover, typical cytometers require relatively large volumes of samples and reagents for quantitative and statistical analysis, further increasing the total cost per each experimental run, thus creating difficulties in realizing certain applications, particularly in point-of-care applications. Each of these concerns limits the full utilization of the benchtop flow cytometer or FACS system in various biomedical and clinical applications, in spite of its powerful capability to rapidly and quantitatively analyze on biological samples at a very high screening throughput.

Lab-on-a-chip microfluidic flow cytometers hold promise to overcome each of the above-mentioned difficulties. The lab-on-a-chip platform makes possible inexpensive, disposable, and portable devices in which many aspects, such as fluidics, optics or acoustics, are highly integrated on a single plastic chip to work synergistically to create novel functionalities that might not have been possible in conventional ways. Their small size and low cost promote portability and affordability by research laboratories and individual clinics.

Numerous studies have indicated that blood transportation time and handling procedure can affect test results significantly [14, 15]; thus on-the-spot test using portable analysis tool can help produce more consistent and reliable results in a very short period time on the spot. Readily transportable devices can be deployed for testing in remote or resource poor locations, such as battlefields or rural areas in Asia or Africa where medical testing is not widely available.

Microfluidic flow cytometers can operate with small amount of sample and reagent volume, thus lowering the cost of assays and running experiments. A mass-producible device would be more widely accessible to both research labs and individual clinics, yielding faster assay turnaround and enabling for much more efficient research. The closed, small-volume platforms would allow safe handling of rare (i.e. precious) cells and infectious biospecimens to be safe from potential cross-contamination or cell loss.

An integrated optical system on a chip would have fewer problems than most current benchtop systems based on off chip bulk optics that require precise alignment. In fact, a highly integrated chip-based approach would turn the time consuming and expensive work of troubleshooting into simple chip replacement; and the probability of hardware failure will be reduced significantly when the optical components are integrated onto a single chip in a pre-aligned manner. This approach should eliminate the need for costly service contracts and dedicated maintenance personnel, which are not usually easily available in underserved or resource-poor areas.

Most importantly, a microfluidic flow cytometer offers the potential for innovative architecture and increased functionality impossible for conventional bench top systems. The high level integration, along with parallel processing techniques, can be exploited for higher throughput screening, even with lower flow speeds. A closed sorting system reduces potential biohazard risks. If combined with the ability to integrate other valuable functionalities like fluid pumping, sample preparation, and cell

culturing, the possibilities for true lab-on-a-chip micro total analysis system (μTAS) development are endless.

Numerous microfluidic cell sorting devices have been explored based on various working principles, including dielectrophoresis[16], magnetophoresis[17], optical gradient forces[18], and hydrodynamic flow switching[19, 20] using external actuators, among others. Of those mechanisms, however, fewer approaches have been proven to meet the requirements for real-life biological or clinical applications, namely high throughput, adequate detection sensitivity, and acceptable sorting accuracy/purity. The high screening throughput about 1000 cells/sec or even higher is required as screening of a large number of cells (more than 1 million cells) is essential in order to identify rare cells in a population or to extract meaningful clinical data out of a small volume of samples for real applications. Many μFACS systems suffer from low throughput (lower than 100 cells/sec) due to the lack of a fast actuation mechanism or a high-speed real-time control system. High detection sensitivity is an essential feature to detect low intensity fluorescence signals from small biomolecules, such as bacteria, and to clearly identify samples of interest. High signal-to-noise ratios allow for simpler and more accurate threshold determination and prevent false/inaccurate sorting, thus enhancing sorting purity. An automated control system is critical to accurate sorting for creating an enriched sample of biospecimens of interest.

While the most advanced microfluidic flow cytometers may not be ready to replace traditional benchtop cytometers in the just clinic yet, the necessary technologies to realize this goal are growing fast, rapidly bridging and even over-reaching the gap

between the commercial benchtop systems and the rapidly developing microfluidic platforms.

Three core components of benchtop flow cytometers/FACS need to be miniaturized while maintaining performance: (1) the fluidic system for introduction and placement of biological samples, (2) the optical system for illumination of samples and collection of emitted light (both scattered and fluorescent), and (3) the sorting system for deflection of samples of interest, which requires both real-time control and a rapid-response actuation system. Another key challenge to developing high-performance miniaturized flow cytometers/FACS is to figure out how to reduce the volume and cost of these three systems while maintaining adequate performance (e.g. detection sensitivity and sorting throughput).

1. 3. Thesis overview

This thesis discusses a few important achievements on developing microfluidic lab-on-a-chip platform flow cytometers and FACS focusing on integrating optics, acoustic actuators and also miniaturizing the whole peripheral detection system.

Chapter 2 will discuss thy typical polydimethylsiloxane (PDMS) related fabrication process including the process of Teflon AF coating on the microfluidic wall.

Chapter 3 will introduce a novel way of on-chip illumination employing Teflon AF-coated optofludic waveguides. Light introduced into the microfluidic channel by an optical fiber is confined to and guided along the long microfluidic channel, thus enhancing the detection sensitivity. It also enables for multi-spot illumination and detection, which are key factors to the 'space-time' and 'color-space-time (COST)' technologies, which will be explained in detail in Chapter 4 and Chapter 5, respectively. Chapter 3 or portion thereof has been published in *IEEE Photonics Technology Letters* 2009, S. H. Cho, J. M. Godin, and Y.-H. Lo.

Chapter 4 will introduce a high-throughput microfabricated fluorescence-activated cell sorting system employing an on chip integrated piezoelectric actuator. Fabricating the device with the on-chip optical system and the real-time control system will be discussed in detail. Enhancement in detection sensitivity is achieved by (1) 'space-time' coding technology, and (2) finite-impulse-response (FIR) match filter

algorithm. Moreover, its real application to biomedical research in sorting mammalian cells and e-colis is demonstrated as well. Chapter 4 or portion thereof has been published in *Lab on a Chip* 2010, S. H. Cho, C.-H. Chen, J. M. Godin, F. S. Tsai, and Y.-H. Lo.

Chapter 5 will show an important milestone in realizing point-of-care applications of microfluidic flow cytometer and FACS. A novel fluorescent detection technique employing 'color-space-time (COST)' coding technique enables to discriminate up to eleven fluorescent colors using only a single PMT, thus enabling significant reduction in cost and size of the whole optical detection system. Chapter 5 or portion thereof has been published in *Applied Physics Letters* 2010, S. H. Cho, W. Qiao, F. S. Tsai, K. Yamashita, and Y.-H. Lo.

Chapter 6 will summarize the thesis and briefly mention future works.

Appendix will introduce a new technique to fabricate aspherical polymer lens using tunable liquid-filled mold. The fabrication process and the profile measurement setup and analysis on aspherical profiles of PDMS lenses are discussed. Appendix or portion thereof has been published in *Optics Letters* 2009, S. H. Cho, F. S. Tsai, W. Qiao, N.-H. Kim, and Y.-H. Lo.

References:

1. A. Givan, *Flow cytometry: first principles*. (John Wiley & Sons, 2001).

2. H. Shapiro and R. Leif, *Practical flow cytometry*. (Wiley-Liss New York, 2003).

3. A. Lehmann, S. S¯rnes and A. Halstensen, Journal of immunological methods **243** (1-2), 229-242 (2000).

4. R. Nunez, Current issues in molecular biology **3**, 67-70 (2001).

5. P. Pala, T. Hussell and P. Openshaw, Journal of immunological methods **243** (1-2), 107-124 (2000).

6. M. Roederer, J. Brenchley, M. Betts and S. De Rosa, Clinical immunology **110** (3), 199-205 (2004).

7. J. Gratama, A. Orfao, D. Barnett, B. Brando, A. Huber, G. Janossy, H. Johnsen, M. Keeney, G. Marti and F. Preijers, Cytometry Part B: Clinical Cytometry **34** (3), 128-142 (1998).

8. C. Jennings and K. Foon, Blood **90** (8), 2863 (1997).

9. C. Jennings and K. Foon, Cancer Investigation **15** (4), 384-399 (1997).

10. P. Chattopadhyay, D. Price, T. Harper, M. Betts, J. Yu, E. Gostick, S. Perfetto, P. Goepfert, R. Koup and S. De Rosa, Nature medicine **12** (8), 972-977 (2006).

11. S. De Rosa, L. Herzenberg and M. Roederer, Nature medicine **7** (2), 245-248 (2001).

12. D. Godfrey, S. Kinder, P. Silvera and A. Baxter, Journal of Autoimmunity **10** (3), 279-285 (1997).

13. A. Risitano, H. Kook, W. Zeng, G. Chen, N. Young and J. Maciejewski, Blood **100** (1), 178 (2002).

14. R. Dickover, S. Herman, K. Saddiq, D. Wafer, M. Dillon and Y. Bryson, Journal of clinical microbiology **36** (4), 1070 (1998).

15. M. Keeney, I. Chin-Yee, R. Nayar and D. Sutherland, Journal of Hematotherapy **8** (4), 327-329 (1999).

16. J. Voldman, M. Gray, M. Toner and M. Schmidt, Anal. Chem **74** (16), 3984-3990 (2002).

17. N. Pamme and C. Wilhelm, Lab on a Chip **6** (8), 974-980 (2006).

18. M. Wang, E. Tu, D. Raymond, J. Yang, H. Zhang, N. Hagen, B. Dees, E. Mercer, A. Forster and I. Kariv, Nature biotechnology **23** (1), 83-87 (2004).

19. H. Bang, C. Chung, J. Kim, S. Kim, S. Chung, J. Park, W. Lee, H. Yun, J. Lee and K. Cho, Microsystem Technologies **12** (8), 746-753 (2006).

20. A. Wolff, I. Perch-Nielsen, U. Larsen, P. Friis, G. Goranovic, C. Poulsen, J. Kutter and P. Telleman, Lab on a Chip **3** (1), 22-27 (2003).

Chapter 1 or portion thereof has been published in *Lab on a Chip*, Sung Hwan Cho, Chun-Hao Chen, Frank S. Tsai, Jessica M. Godin, and Yu-Hwa Lo, vol. 10, 1567 (2010)

Chapter 2

Fabrication of microfluidic flow cytometer and fluorescence-activated cell sorter (μFACS)

In this chapter, fabrication steps making microfluidic flow cytometers and cell sorters are introduced. Two methods of fabricating those microfluidic device master molds will be introduced first; (1) SU-8 photoresist mold process, (2) Cryogenic etching

process. The Teflon AF coated optofluidic waveguide fabrication process and the direct bonding process of the PZT actuator on top of the PDMS chamber are also introduced.

2. 1. SU-8 mold fabrication

The lab-on-a-chip multicolor flow cytometer, COST device and early version of μFACS were fabricated by soft lithography mold replica techniques using SU-8 negative photoresist [1]. In the first, standard UV lithography techniques are used to transfer a pattern including microfluidic channels from a photomask printed on a transparency film at the resolution of 20,000 dpi into roughly 50 μm to 100 μm of SU-8 negative photoresist on a Si wafer. The thickness of the SU-8 film is controlled by the spinning speed with ease and precision.

After development of the unexposed (e.g. non-crosslinked) photoresist, the remaining SU-8 photoresist on the Si substrate forms the microfluidic device features on the Si wafer, such as fluidic channels, two-dimensional lenses and waveguides channels etc. Subsequent hard baking for 1 hour at 200 ^{o}C enhances robustness of the mold.

The SU-8 mold is then ready for PDMS replica molding process that is discussed in section 2. 4. The mold master is silanized by vapor deposition of trichlorosilane (TCI Inc., USA) to facilitate PDMS demolding process.

2. 2. Si mold fabrication by cryogenic etching process

The high aspect ratio of the channel (>1:10) at the sorting junction requires a robust and vertical channel wall structure. To meet these requirements, the Si mold

masters are fabricated by the cryogenic reactive ion etching (RIE) process at -115 ^{o}C [2]. Microfluidic channels and sorting chambers are photolithographically defined using S-1805 positive photoresist (Shpley, USA). A film of 50 nm thick nickel is evaporated onto the device pattern made of the photoresist followed by the lift-off process, to serve as an etch mask during the following low temperature dry-etching process. The Si mold master (~100 μm deep) is etched at -115 ^{o}C using ICP-assisted reactive ion etching (ICP RIE; Plasmalab 100, Oxford Instruments). A plasma ignited from a mixture of O_2 and SF_6 gases at 12 mTorr performs the vertical etching and sidewall passivation simultaneously, resulting in smooth and very vertical channel walls [3]. Etching rates are usually on the order of 120 μm per hour. After the RIE process, the nickel mask is removed with nickel etchant, and the Si mold is ready for the PDMS replica molding process after being silanized.

2. 3. Teflon AF coating process

The novel light guiding architecture, where the excitation laser light shares the same physical path with the biological samples flowing in the fluidic channel, is created by coating amorphous Teflon (Teflon AF, DuPont Inc.) onto the channel wall [4]. Teflon AF is a fluoropolymer with a refractive index (n=1.31) lower than that of water (n=1.33), so that it forms a cladding layer while water becomes a core of the optofluidic waveguide. While most fluoropolymers are opaque or translucent, Teflon AF is optically transparent to UV and visible light[5].

To achieve a uniform Teflon AF coating layer along the microfluidic channel, 2% Teflon AF solution was injected first, and channel outlets are exposed to a slight negative pressure (P = -10 kPa) for 20 min. The balance between the vacuum pressure applied and the adhesion of Teflon AF to the PDMS channel wall determines the thickness of the Teflon AF layer. The device is then heated up to 175 ^{0}C that is 15^{0}C above the glass temperature of Teflon AF to obtain a smooth layer[6]. The detailed fabrication process will be further discussed in Chapter 3.

2. 4. Fabrication of μFACS

PDMS prepolymer (Sylgard 184, Dow Corning) mixed with curing agent at 1:10 ratio is poured onto the SU-8 or Si mold and cured thermally in the oven for 2 hours at ~ 65 ^{o}C. The PDMS layers are then peeled off of the molds after being cured, and holes for any sample inlets/outlets, and biopsy punchers punch actuation chambers. Another PDMS layer without any pattern on it is ready in a similar way. Both of the PDMS surfaces are treated by the UV/Ozone process in order to facilitate strong covalent bonding between the top and the bottom PDMS layer, and finally forming closed microfluidic channels and actuation chambers.

The stainless steel surface of the PZT actuator is polished with 1μm alumina particle (Buehler Inc., USA) until a mirror-like surface is obtained. The polished stainless steel surface is cleaned and then UV-Ozone treated to facilitate direct bonding to a sorting chamber of the PDMS device. The direct bonding process of stainless steel surface and PDMS is completed after ~ 4 hours in an 85 ^{o}C oven. The strong bonding

between the polished stainless steel and PDMS chamber keeps fluid from leaking even under the relatively high flow velocity (e.g. 10 cm/sec), and it also guarantees excellent actuation power coupling between the actuator and the fluid.

References:

1. X. Zhao, Y. Xia and G. Whitesides, Journal of Materials Chemistry **7** (7), 1069-1074 (1997).

2. M. Boer, J. Gardeniers, H. Jansen, M. Gilde, G. Roelofs, J. Sasserath and M. Elwenspoek, Journal of microelectromechanical systems **11** (4), 385-401 (2002).

3. J. Godin, S. H. Cho and Y.-H. Lo, oecc2009.org, 1-2 (2009).

4. S. Cho, J. Godin and Y. Lo, IEEE Photonics Technology Letters **21** (15), 1057 (2009).

5. J. Lowry, J. Mendlowitz and N. Subramanian, 1991 (unpublished).

6. S. H. Cho, J. Godin and Y.-H. Lo, IEEE PHOTONICS TECHNOLOGY … (2009).

Chapter 3

Optofluidic waveguides in Teflon AF-coated PDMS microfluidic channels for enhancing detection sensitivity

In this chapter, we discuss a new method for fabricating an optofluidic (i.e. liquid-core) waveguide that is compatible with PDMS replica molding process. The light path follows the microfluidic channels, and architecture that can maximize detection efficiency and make the most economic use of chip area in many lab-on-a-chip

device applications including microfluidic flow cytometry. The PDMS-based microfluidic channels are coated with Teflon amorphous fluoropolymers (Teflon AF), which has a lower refractive index (n = 1.29 ~ 1.31) than that of water (n = 1.33), thus forming a water-core and Teflon AF-cladding waveguide inside microfluidic channels.

Driven by a vacuum pump, the Teflon AF solution was flowed through the microfluidic channels, leaving a thin (5-15 μm) layer of coating on the channel wall as the cladding layer of optofluidic waveguides. This coating process resolves the limitations of spin-coating process by reducing the elasticity mismatch between the Teflon AF cladding layer and the PDMS device body.

We demonstrate that the resulting optofluidic waveguide confines and guides the laser light through the liquid core channel. Furthermore, the light in such a waveguide can be split when the fluid flow is split. This new method enables highly integrated biosensors such as lab-on-a-chip flow cytometers and micro-fabricated fluorescence-activated cell sorter with on-chip excitation.

3. 1. Introduction

Optofluidics has been an emerging field that integrates microfluidics and optics on the same device to work synergistically to create novel functionalities in a tiny device [1, 2]. Devices that contain both microfluidic channels and on-chip (2-dimensional) photonic circuits, such as integrated biochemical sensors, show enhanced functionality and sensitivity and enable significant cost and size reduction.

Many researcher groups have demonstrated that fluidic channels and optical waveguides can be fabricated on the same substrate [3, 4]. In order to assure that photons and biological samples such as cells in the fluid interact most effectively for the highest detection sensitivity, however, we desire the flexibility to direct and align the paths of light and fluid. In some cases, we need light beams to intersect the fluidic channels to localize the interrogation are [5, 6]. In other cases, we want the light wave and the fluid to share the same path to maximize their interaction. For the latter case, we still lack an effective fabrication method. Due to the fact that most polymers used in lab-on-a-chip devices have a higher index of refraction than water, light traveling in the fluidic channel will not be confined, suffering from high radiation loss.

Wolfe et al created a liquid-core and liquid-cladding (L2) waveguide structure by using higher refractive index solution (n>1.4) as a sample flow and as a core of the waveguide, while water (n=1.33) forms a cladding layer of the optofluidic waveguide [7]. In a similar way, a liquid-core and air-cladding waveguide structure was also studied[8]. These liquid-core waveguides, however, have several limitations to be practically used for general lab-on-a-chip applications. First of all, both of the waveguide structures lack of 3-dimensional light confinement, as the fluid is focused only two dimensionally, thus resulting in serious light radiation loss along z-axis. The high refractive index solution used for the liquid-core might not biologically compatible, and the external vacuum pump is required to form the air-cladding layer.

In this chapter, we report a polydimethylsiloxane (PDMS)-compatible process of coating microfluidic channels with a layer of low refractive index Teflon amorphous

fluoropolymer (Teflon AF) solution, enabling the water in the fluidic channel to be used as the waveguide's high index core. We further show that the Teflon AF-coated waveguide works not only for straight fluidic channels but also for split channels. In addition to delivering the light, by Teflon coating the microfluidic channel, we also create a channel with low sample adsorption, avoiding a troublesome problem found in many polymer-based microfluidic devices.

3. 2. On-chip optofluidic waveguides using Teflon AF

Teflon AF is an amorphous fluoropolymer that is chemically stable and optically transparent from ultraviolet (UV) to infrared wavelengths. Unlike other fluoropolymers such as PTFE, Teflon AF has a refractive index (n=1.29 ~ 1.31) that is lower than the index of water (n=1.33); therefore, a Teflon AF coating layer on PDMS microfluidic walls can be used to clad a liquid-core optical waveguide. Light will then be delivered through the same physical path as the fluid flows by total internal reflection when the coated channels are filled with water or aqueous solutions.

Datta *et al*. reported the fabrication of Teflon AF-coated liquid core waveguides by spin-coating a Teflon AF solution onto silicon or glass substrates [9, 10]. The fabrication process with silicon or glass substrate, however, is relatively expensive and time consuming, which is not desirable for low-cost lab-on-a-chip applications. If the Teflon AF coating process can be applied to polymer such as PDMS as illustrated in Figure 3.1, a favored material for developing many of today's microfluidic devices, it can be an attractive process for use in lab-on-a-chip devices.

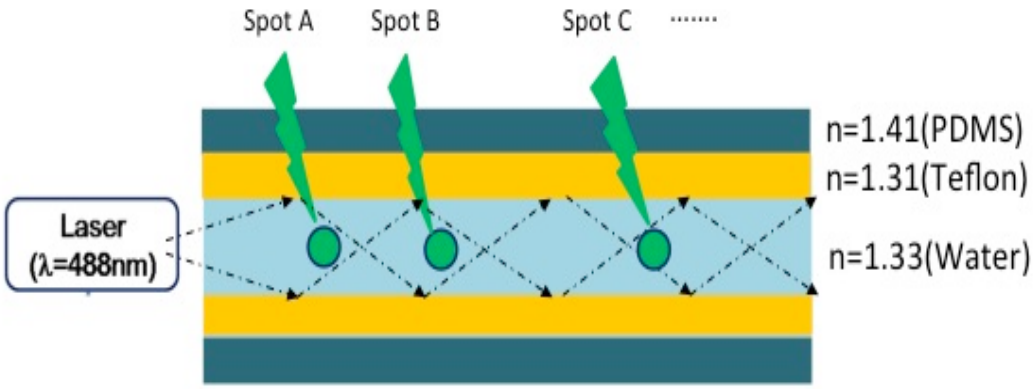

Figure 3.1 Schematic of Teflon AF coated optofluidic waveguide inside microfluidic channel made of PDMS. The Teflon AF coating layer has lower refractive index than that of water flowing along the microfluidic channel; illumination light is confined to the microfluidic channel by total internal reflection. Light is guided along the liquid-core waveguide, thus enabling to detect fluorescence signals at multiple locations.

Guo *et al.* fabricated a Teflon AF-coated liquid core waveguide by spin-coating Teflon AF on PDMS substrates[11]. However, the spin coating of Teflon AF onto a PDMS substrate has several limitations in fabrication process. One challenge of the spin-coating process is that once the Teflon AF coating is formed on PDMS substrates, bonding between Teflon AF layers on both of the PDMS substrates becomes very difficult, as Teflon AF (like any other Teflon material) is chemically stable. Bonding between Teflon AF coating layers was reported by using physical clamping at temperatures above 330 ^{o}C [11]. At such a high temperature, however, PDMS (e.g.

Sylgard 184) turns brown and loses its optical transparency. In addition surface cracking often results during device process and handling, as the elastic modulus of Teflon AF is about 1,000 times that of PDMS[12].

In order to resolve aforementioned limitations, we demonstrate a new procedure for coating Teflon AF onto the PDMS channel walls by flowing Teflon AF solution through the microchannel, thereby creating the cladding layer for an optical waveguide along the path of fluid flow. The light introduced to micro channels is confined inside the core of the waveguide (i.e. microfluidic channel) and guided by fluid flowing through the channel.

3. 3. Fabricating Teflon-AF cladding layer

Microfluidic channels that are 200 μm by 70 μm are fabricated in PDMS by soft lithography followed by replica molding process as already explained in Chapter 2. A master mold is lithographically defined on a Si wafer using SU-8 50 (MicroChem). Two replicas are then created: one replica with microfluidic channels and one replica of an optically smooth blank Si wafer. A solution of 2% 1H,1H,2H,2H-perfluorodecyltriethoxysilane (Sigma Aldrich Inc.) is spin-coated onto PDMS substrates and heated at 100 ^{o}C for 10 min to promote adhesion between PDMS and the Teflon AF solution. Both PDMS surfaces are then activated for permanent bonding by UV/Ozone treatment (UVO-CLEANER 42, Jelight Inc.) for 3 min and bonded together, thus capping the microfluidic channels. A 6% Teflon AF solution (601-S2, DuPont Corp) is flowed into the microfluidic channels. Once they are filled, vacuum (P=-20 kPa) is

applied for 20min to remove excess Teflon AF solution from the channels as illustrated in Figure 3.2. The balance between the vacuum force and the adhesion to the PDMS channel wall determines the thickness of the cladding layer.

The process results in a smooth channel with a hollow core. The Teflon AF-coated PDMS device is heated to 155 ^{o}C for 20 min to evaporate the fluoroinert solvent, and then heated further to 175 ^{o}C (15 ^{o}C above its glass transition temperature) for 20 min to form a smooth Teflon AF layer. This relatively low temperature coating is compatible with the PDMS process while significantly reducing the consumption of Teflon solution compared to the spin-coating process. Calculations show that a ~ 5μm thick Teflon AF film is necessary to confine the light to the liquid core [13].

In our work, the cladding thickness is typically 5 ~ 15 μm, thick enough to confine and guide light waves. The thickness of the Teflon AF coating layer can be further controlled by adjusting the applied vacuum pressure and concentration of the Teflon AF solution. After slowly cooling the devices to avoid cracking due to thermal mismatch, an optical fiber is inserted into the channel for light coupling. Deionized (DI) water is then introduced into the hollow core to serve as both the sample flow carrier and the core of the optofluidic waveguide carrying photons as well. Figure 3.2 below illustrates the fabrication process of the Teflon AF coated optofluidic waveguide schematically.

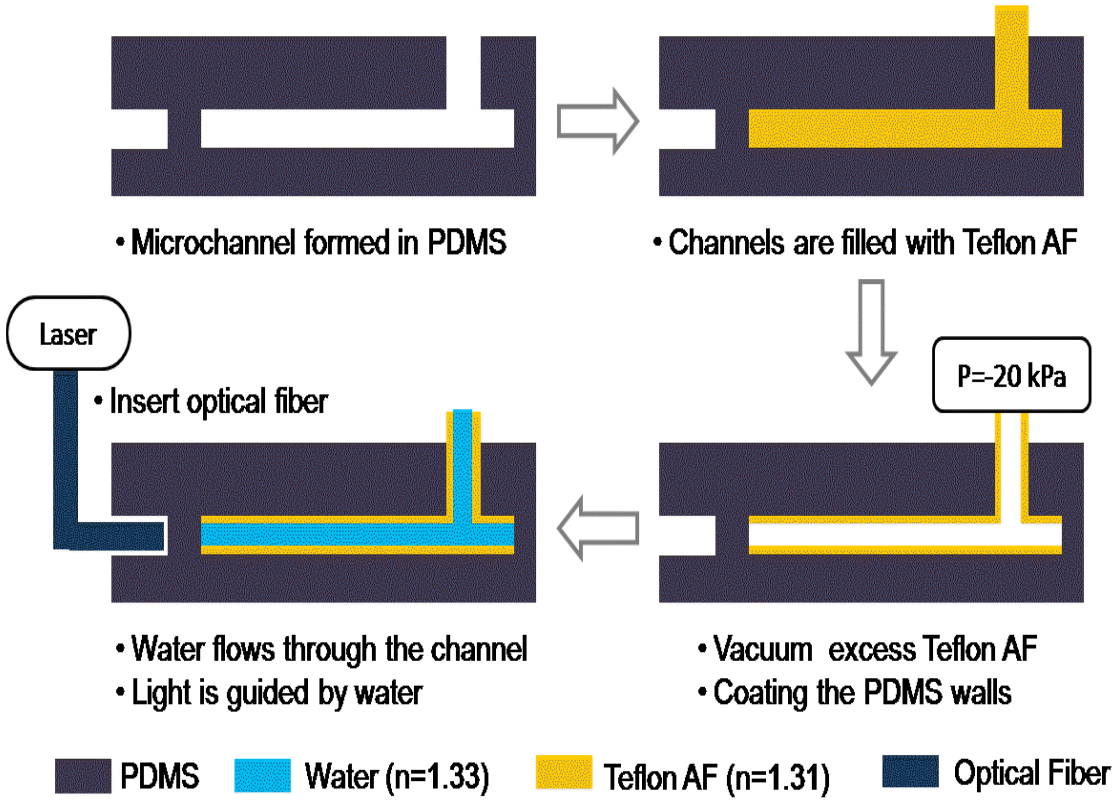

Figure 3.2 Fabrication process for Teflon-AF coated liquid core waveguides. This process reduces the elastic mismatch between PDMS and Teflon AF, enabling the coating process to be compatible with common PDMS fabrication process. The final thickness of the Teflon AF coating layer is controlled by the applied vacuum pressure and concentration of Teflon AF solution to start with.

3. 4. Teflon AF coated optofluidic waveguide

The flowing DI water transports both the suspended samples and the light in the same channel. The numerical aperture, NA = $(n^2_{core} - n^2_{cladding})^{1/2}$, of the liquid core waveguide is 0.23, well matched to the NA of the input multimode fiber (NA=0.22). The cross section of the liquid core waveguide is imaged by a charged coupled device at the end of the channel, as shown in Figure 3. 3 (a). Figure 3. 3 (b) shows the cross section of the fabricated microfluidic channel that is 200 μm by 70 μm. Figure 3.3 (c) shows the light output of the optofluidic waveguide when the laser is ON. The dotted box shows the wall of the PDMS channel, and the solid line shows the boundary between the Teflon AF cladding layer and the liquid core. It verifies that the light is confined to the liquid core of the optofluidic waveguide by the Teflon AF coating. A waveguide loss of 2.13 dB/cm at 488-nm wavelength is measured. Scattering at the surface of the Teflon AF layer is the dominant factor for the relatively high light loss compared to light leakage and absorption. With improved smoothness of Teflon AF coating, we believe the waveguide loss can be reduced significantly.

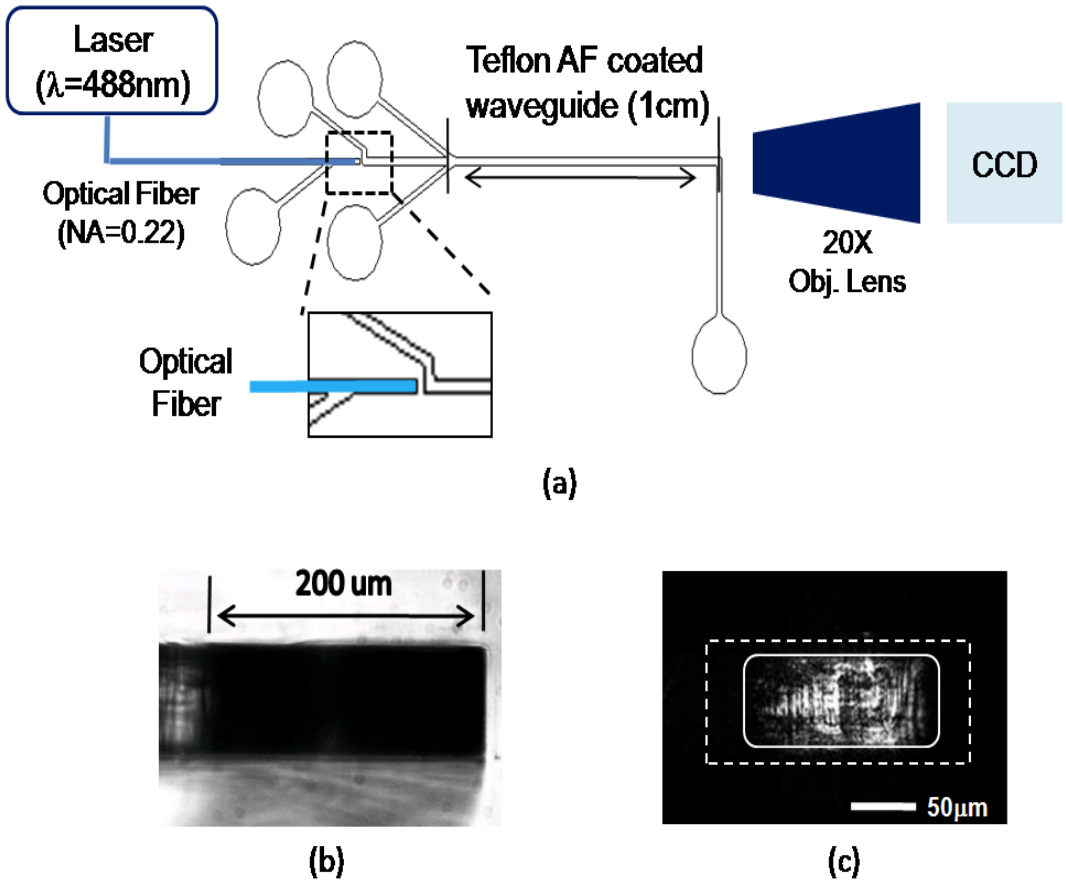

Figure 3.3 (a) Experimental setup for light output measurement. (b) Cross section of the liquid core waveguide. (c) Light from a liquid core waveguide with Teflon AF coating. The dotted box is the perimeter of the channel, and the solid line is the Teflon AF-coated core layer. It is clearly seen that introduced laser light by the optical fiber is well confined to the core of the optofluidic waveguide.

Figure 3.4 (a) shows the layout of a microfluidic channel which includes a splitting junction, and Figure 3.4 (b) is a photograph of the device. Laser light (λ = 488 nm) is fiber-coupled into the microfluidic channel, in which wafer flows with biological samples. Light is guided by the fluid flow by total internal reflection, and at the three-way junction, as shown in the enlarged box in Figure 3.4 (a), the 488 nm light is divided into three paths following the fluid flow towards the channel outlets.

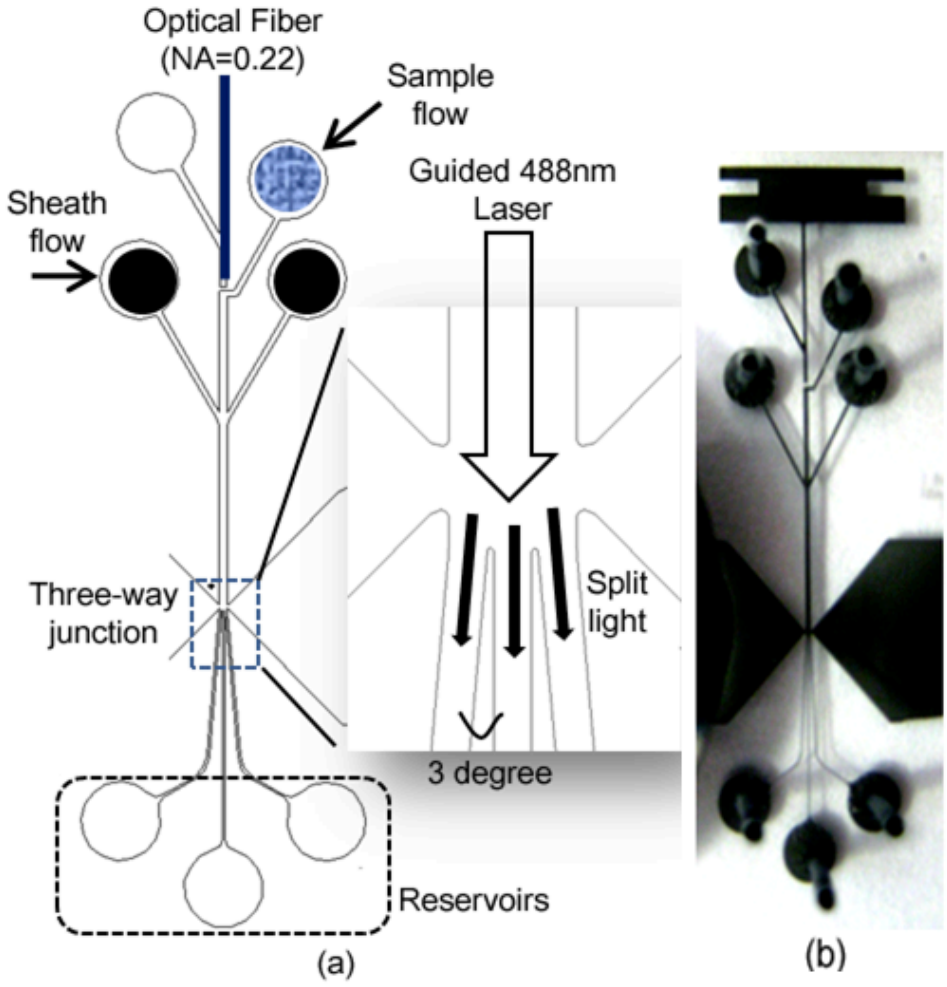

Figure 3.4 (a) Layout of the device. Light can be split and guided at the three-way junction. (b) Photography of the device fabricated in PDMS. All the channels and chambers are filled with blackened PDMS for visualization.

In order to demonstrate that light can be split and guided through three sorting channels after the main channel is split, we have first filled the device with a diluted Rhodamine 6G solution that emits green fluorescence in all directions after absorption of the guided 488 nm laser light. As shown in Figure 3.5, the light guided from the upstream channel is divided into three split channels separated by three degree. The result demonstrates that the excitation light is split into three sub channels and that the split light is still guided through the channels. Figure 3.6 shows that excitation light traces fluorescent beads along the entire microfluidic channel, even after the main channel is split into three sorting channels.

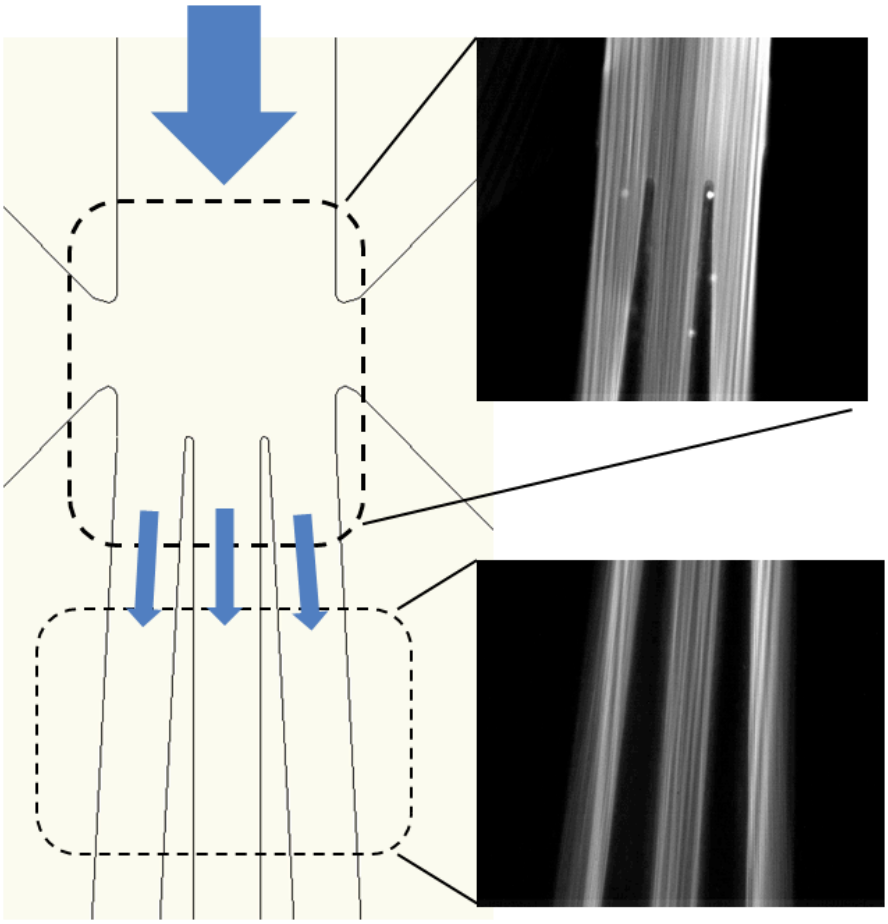

Figure 3.5 Light emitted by Rhodamine 6G when the 488 nm laser sharing the same paths as the fluid excites the fluorescent dye in the fluid. We show that the 488-nm input light is guided through the entire paths of fluidic channels.

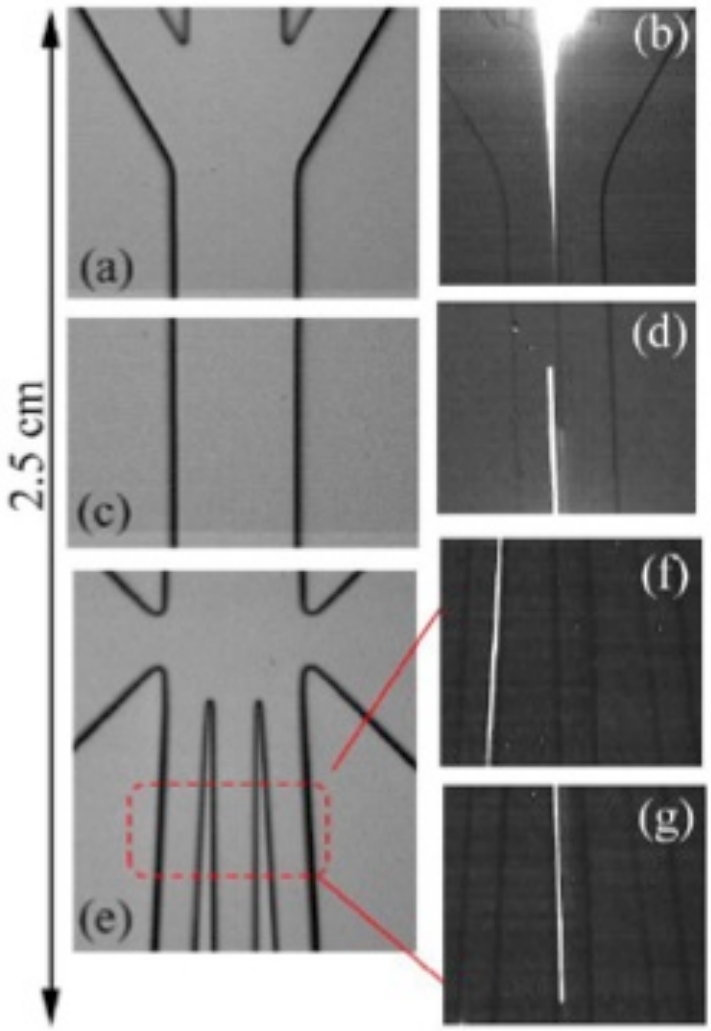

Figure 3.6 Light emitted by polystyrene fluorescent beads (Dragon Green, emission peak at 520 nm). Confined and guided excitation light traces fluorescent beads from the beginning of the sample channel (a, b), even after the channel is split into three sorting channels (e, f, g). As the fluidic channel is split, so is the light.

Since the light always traces the fluid flow in which samples are suspended, excitation is performed at all locations, and thus detection can be performed at any position. This unique property provides a very convenient feature for lab-on-a-chip devices. For example, it becomes possible to perform highly sensitive fluorescence detection at multiple locations using only one single laser, imparting a high degree of design flexibility to miniaturized optofluidics devices, such as lab-on-a-chip flow cytometers or micro-fabricated fluorescent-activated cell sorter (μFACS).

3. 5. Conclusion

To summarize, we have developed a new fabrication process for shared-path optofluidic waveguides by using Teflon AF to selectively coat the microfluidic channels of our choosing. We choose Teflon AF for its low refractive index relative to water and for its optical transparency. Our new Teflon AF coating process is compatible with PDMS that is one of the most popular polymers in microfluidics in that the process removes the elasticity mismatch between Teflon AF and PDMS and preserves both the optical and physical properties of PDMS that make it desirable for many microfluidic applications.

In addition, the process requires only a small amount of Teflon AF solution (less than 20 μl). This enables optofluidic waveguides to be fabricated in PDMS in a cost-effective, less time-consuming manner. The coating layer created by our new process is tunable via adjustment of the dilution (viscosity) of the Teflon AF solution and also by force applied by the vacuum. Furthermore, we demonstrate that as the fluid path is split,

so is the light path, creating a fluidically controlled optical circuit. This technology offers design flexibility and efficient interactions between light and samples for lab-on-a-chip devices. Two important applications of the proposed Teflon AF optofluidic waveguides will be discussed further in the following chapters. Space-time coding and color-space-time (COST) coding technology will be introduced in Chapter 4 and Chapter 5, respectively.

References:

1. C. Monat, P. Domachuk and B. Eggleton, Nature Photonics **1** (2), 106-114 (2007).

2. D. Psaltis, S. Quake and C. Yang, Nature **442** (7101), 381-386 (2006).

3. D. Chang-Yen, R. Eich and B. Gale, Journal of Lightwave Technology **23** (6), 2088 (2005).

4. V. Lien, Y. Berdichevsky and Y. Lo, IEEE Photonics Technology Letters **16** (6), 1525-1527 (2004).

5. J. Godin, S. H. Cho and Y.-H. Lo, oecc2009.org, 1-2 (2009).

6. J. Godin, V. Lien and Y. Lo, Applied Physics Letters **89**, 061106 (2006).

7. D. Wolfe, R. Conroy, P. Garstecki, B. Mayers, M. Fischbach, K. Paul, M. Prentiss and G. Whitesides, Proceedings of the National Academy of Sciences of the United States of America **101** (34), 12434 (2004).

8. J. Lim, S. Kim, J. Choi and S. Yang, Lab on a Chip **8** (9), 1580-1585 (2008).

9. A. Datta, I. Eom, A. Dhar, P. Kuban, R. Manor, I. Ahmad, S. Gangopadhyay, T. Dallas, M. Holtz and H. Temkin, IEEE sensors journal **3** (6), 788-795 (2003).

10. R. Manor, A. Datta, I. Ahmad, M. Holtz, S. Gangopadhyay and T. Dallas, IEEE sensors journal **3** (6), 687 (2003).

11. C. Wu and G. Gong, IEEE sensors journal **8** (5), 465 (2008).

12. J. Làtters, W. Olthuis, P. Veltink and P. Bergveld, Journal of Micromechanics and Microengineering **7**, 145 (1997).

13. P. Dress, M. Belz, K. Klein, K. Grattan and H. Franke, Sensors and Actuators B: Chemical **51** (1-3), 278-284 (1998).

Chapter 3 or portion thereof has been published in *IEEE Photonics Technology Letters*,

Sung Hwan Cho, Jessica M. Godin, and Yu-Hwa Lo, 21 (15), 1057 (2009)

Chapter 4

Highly integrated microfabricated fluorescence-activated cell sorter (μFACS) for sorting a variety of biological samples

We demonstrate a high performance microfabricated FACS system with highly integrated microfluidics, optics, acoustics, and electronics. Single cell manipulation at a high speed is made possible by the fast response time (~0.1 msec) of the integrated PZT actuator and the nozzle structure at the sorting junction. A Teflon AF-coated optofluidic

waveguide along the microfluidic channel guides the illumination light, enabling multi-spot detection, while a novel space-time coding technology enhances the detection sensitivity of the μFACS system. The real-time control loop system is implemented using a field-programmable-gate-array (FPGA) for automated and accurate sorting.

The μFACS achieves a high purification enrichment factor: up to ~230 fold for both polystyrene beads and suspended human mammalian cells (K562) and E.colis at a high throughput (>1000 cells/sec). The sorting mechanism is independent of cell properties such as size, density, and shape, thus the presented system can be applied to sort out any pure sub-populations. This new lab-on-a-chip FACS system, therefore, holds promise to revolutionize microfluidic cytometers to meet cost, size and performance goals.

4. 1. Introduction

In this chapter, an μFACS system is demonstrated with several unique technical merits, including:

1. High throughput (> 1000 cells/second)
2. Single cell manipulation capabilities
3. Low voltage (10 V_{p-p}), low power (~ 1mW) cell sorting
4. Sorting performance independent of cell's properties
5. High sensitivity through real-time signal amplification
6. High speed real-time electronic control system

The device operates by integrating microfluidics, optics, and acoustics in conjunction with an innovative space-time coding technology and a real-time control system. The universal μFACS can separate any targeted biological samples flowing through the channel regardless of their physical or chemical properties such as size, density, shape, or dielectric properties. Using our sorter, 10 μm polystyrene beads, larger human mammalian cells, and even smaller e-colis (less than 1 μm) were successfully sorted and purified with consistent enrichment factors.

The integrated piezoelectric lead-zirconate-titanate (PZT) actuator hydrodynamically manipulates sub-nanoliter volumes of fluid in which a single cell is suspended. The integrated PZT actuator has a much faster response time (about 0.1 msec) than any off-chip control valve [1, 2]. Such a fast response time minimizes the flow disturbance after isolating targeted cells, allowing single cell manipulation. Besides its fast response time, the PZT actuator is directly mounted on the fluidic chamber, enabling low power (<1mW) and low voltage (<10V peak-to-peak) operation. This integration helps make the sorting system portable, cost-efficient, and disposable for applications like point-of-care diagnostics.

The detection sensitivity of the system is enhanced by the space-time coding technology to be elucidated later in this chapter. The technique of space-time coding requires the following hardware and software components: (1) Teflon AF coated optofluidic waveguides (Chapter 3)[3], (2) a finite-impulse-response (FIR) matched filter algorithm, and (3) specially designed spatial filters that modulate the input fluorescent signals of the biological samples.

The optofluidic waveguide created by coating amorphous Teflon to the channel wall confines light to the microfluidic channels that contain fluorescently tagged biological samples such as cells, bacteria etc. Since the excitation laser light and the cells have the same path of travel, the design produces high excitation efficiency, and most important of all, supports optical detection at multiple locations without suffering from power splitting loss, as already explained in Chapter 3.

Multi-point detection of the same fluorescent emission is the key to the space-time coding technology. Spatial filters with specifically designed slits modulate the emitted fluorescent signals before they reach the detector, and an FIR matched filter algorithm selectively amplifies only the signals while suppressing system noise, thus enhancing the signal-to-noise ratio.

An embedded, closed-loop field-programmable-gate-array (FPGA) control system was developed in order to control the sorting in a real-time, automated fashion. The real-time operating system detects incoming signals, makes a sorting decision, and triggers the PZT actuator at the proper time with a timing jitter under 10 μs. This precise timing control avoids sample loss (i.e. missing rare cells) and sorting mistakes (i.e. accidently sort the non-targeted cells), resulting in high purity enrichment.

We successfully sorted fluorescent 10 μm polystyrene beads out of a mixed solution of fluorescent 10 μm beads and non-fluorescent 5 μm beads with an initial mixture ratio of ~ 1:150. Fluorescent 10 mm beads (i.e. the samples of interest) were purified with an enrichment factor of nearly 200 fold at a high throughput of ~ 1500 beads /sec. Using the same sorting system, human erythroleukemic cells were purified

with an enrichment factor of 230 fold at a high throughput of about 1000 cells/sec. Even smaller E.colis were successfully sorted under the similar experimental conditions with a consistent enrichment factor of ~ 225 fold. This manifested the fact that this micro sorter's operation is not dependent on any physical or chemical properties of samples.

4. 2. Piezoelectric cell sorting mechanism

The PDMS based μFACS device has a 250 μm wide main microfluidic channel followed by a sorting junction (100 μm long) and three sorting channels (80 μm wide each) as shown in Figure 4. 1. The center channel is for collecting unwanted cells and the left and the right channels are for collecting the targeted cells. The integrated piezoelectric actuator on the sorting chamber has a lead-zirconate-titanate (PZT)-stainless steel bimorphous structure, and it bends upward or downward according to the polarity of the applied voltage. If no cell of interest is registered, the PZT does not bend at all, and cells pass through the center waste channel. The operation principle is schematically illustrated in Figure 4. 2.

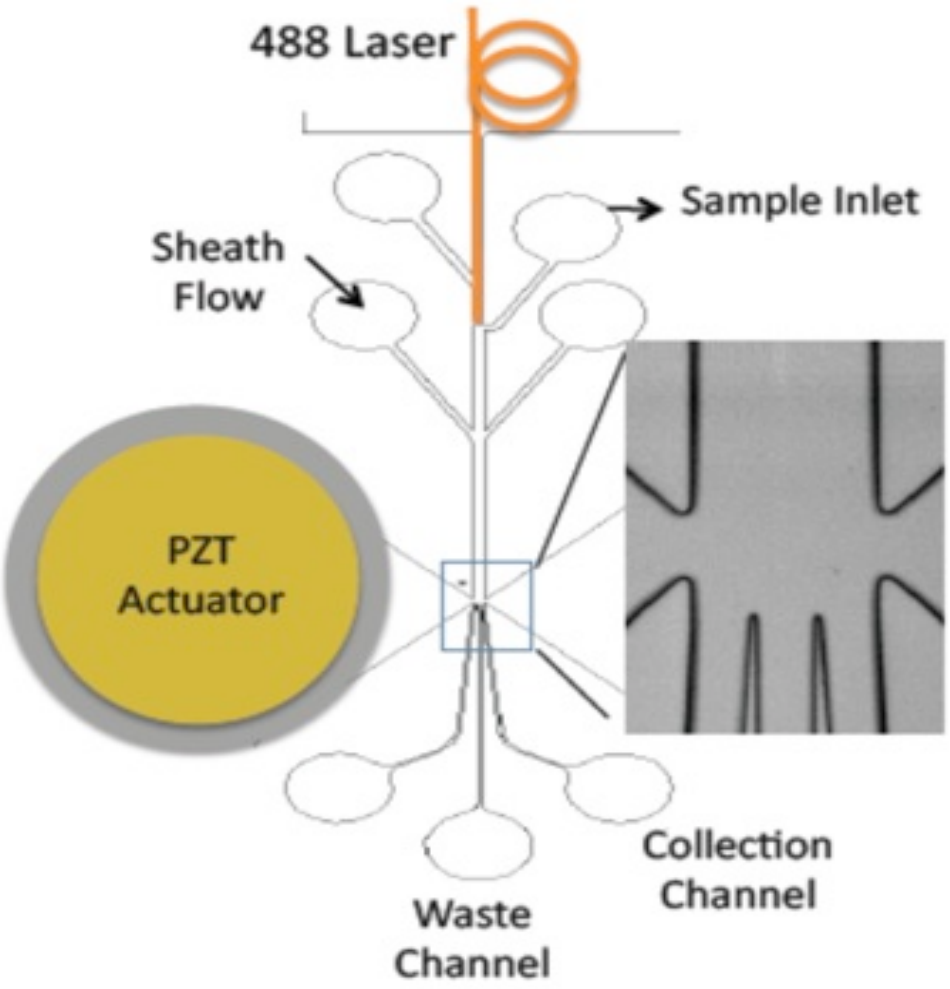

Figure 4.1 Device structure. The 250 μm wide main fluidic channel is split into three sub-channels. The center channel is for collecting waste, while the left and the right channels are for collecting samples. The illumination light (488 nm laser) is delivered to the device by the optical fiber and guided by the Teflon AF coated optofluidic waveguide. The PZT actuator is integrated on the device. In the square is the sorting junction of the device made of PDMS.

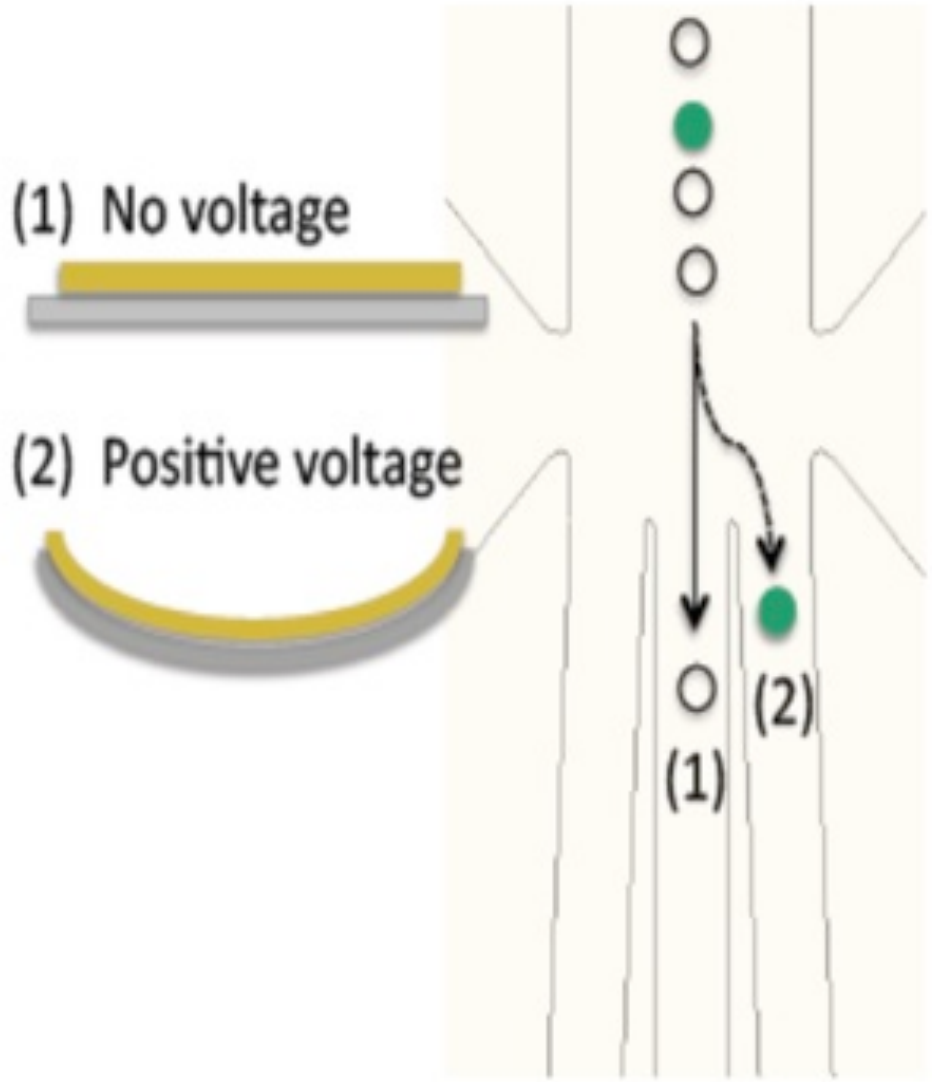

Figure 4.2 As the PZT actuator bends down, the cell of interest is pushed to the right sorting channel, while the non-targeted cell travels directly to the center waste channel without triggering the PZT actuator. The deflection of the PZT disc is precisely controlled by the magnitude and the polarity of the applied voltage.

When the fluorescent light from target cells is registered by the upstream photodetector, the integrated piezoelectric actuator bends according to the voltage pulse applied by the real-time control system and deflects the fluid stream to one of the sorting channels as shown in Figure 4. 3. The exact volume of fluid displacement by the PZT actuator can be precisely controlled by the amplitude of the applied voltage. The bending of the PZT actuator induces a transverse displacement of fluid, typically on the order of sub-nanoliter per each stroke, in less than 0.1 msec. Such a fast actuation speed minimizes the fluid disturbance after firing so that the sorting system exhibits single cell manipulation capabilities with a high throughput.

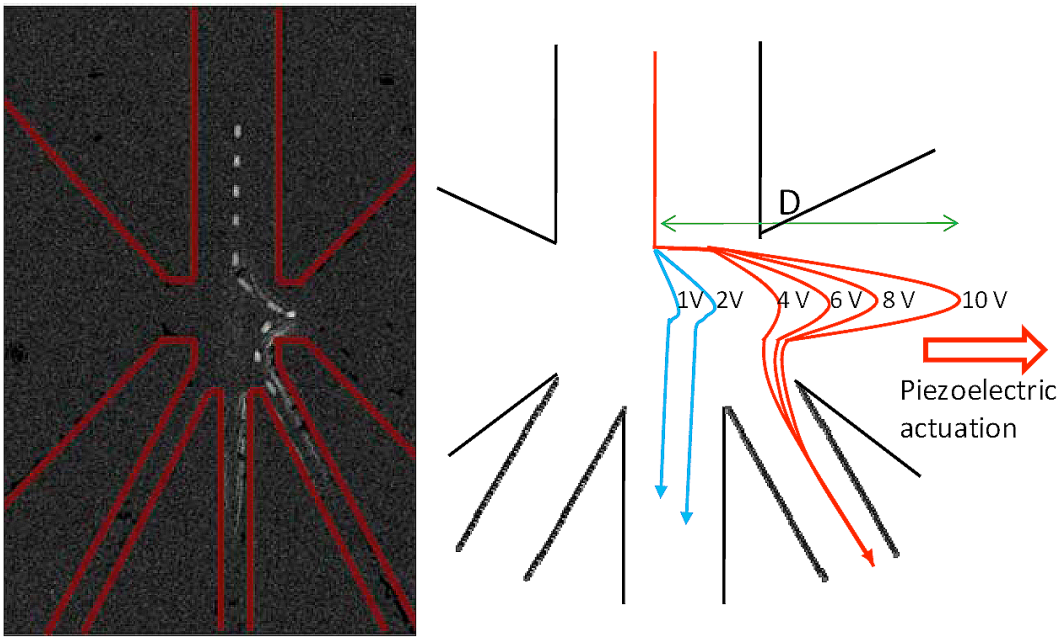

Figure 4.3 Flow pattern observation. Left: Trace of a fluorescent bead sorted to the right channel by superimposing photos taken every 0.3 msec using a high-speed CMOS camera. Right: The bead trajectory plot for the bead under different voltage magnitude to the PZT actuator. This helps set the threshold voltage for sufficient deflection.

4. 3. Teflon AF coated optofluidic waveguide

Coating amorphous Teflon onto the microfluidic wall creates the novel light guiding architecture, where the excitation laser light shares the same physical path with the analytes in the fluidic channel, and this method is already elucidated in the previous chapter (Chapter 3).

The confinement of the light to the microfluidic channel carrying the samples increases the light intensity impinging on the cell and, at the same time, keeps the light intensity low enough to avoid photo bleaching. Light is guided inside the fluidic channel even after the channel is split into three sorting channels after the sorting junction. This waveguide architecture greatly simplifies light routing while minimizing propagation losses and enabling multi-point fluorescent detection.

Besides its light guiding capability, the Teflon AF coated optofluidic waveguide also prevents cells from sticking to the channel walls, which would cause clogging of the fluidic channel, because Teflon AF has low surface energy like other Teflon materials. With reduced clogging, the system can run for a long period of time, allowing the sorting of very rare samples. For instance, in the mammalian cell sorting experiment, the μFACS system ran longer than 2 hours under high throughput (> 1000 cells/sec) without significant cell clogging issue. It demonstrates that the system can monitor more than a few million cells per hour for rare events.

4. 4. Design and fabrication of the μFACS chip

The μFACS device was fabricated by the fabrication process described in Chapter 2.

4. 5. Automated sorting control system and signal processing

In order to achieve high throughput and high sample enrichment, the sort decision needs to be made with precise timing and at a high speed. High detection sensitivity is key to the success in sorting target cells and decreasing the chance of false sorting. We have developed a high-sensitivity automated sorting system by employing the techniques of integrated optics, new device architecture, and signal processing. In particular, the novel fluorescence-detection strategy referred to as "space-time coding" is invented, as illustrated in Figure 4. 4 and Figure 4.5.

Figure 4. 4 shows the schematic of the overall μFACS system, which is much simpler and smaller than a bench top system since most optics and cell sorting hardware have been integrated with the microfluidic lab-on-a-chip device. The laser-induced fluorescence from the stained cells is collected by a 20X microscope objective lens with numerical aperture (NA) is 0.40 (Leica, Germany). As the cell (bead) travels at a speed across the optical interrogation zone defined by three narrow slits made of a mask as shown in Figure 4. 5, the fluorescent signals of the cell (bead) detected by the photomultiplier tube (PMT; PMM02, Thorlabs Inc., USA) display a waveform of three distinct peaks. The spacing between the peaks is equal to the space between the slits on

the mask divided by the travel speed of the cell (bead) and the magnification factor (= 20 for 20X objective).

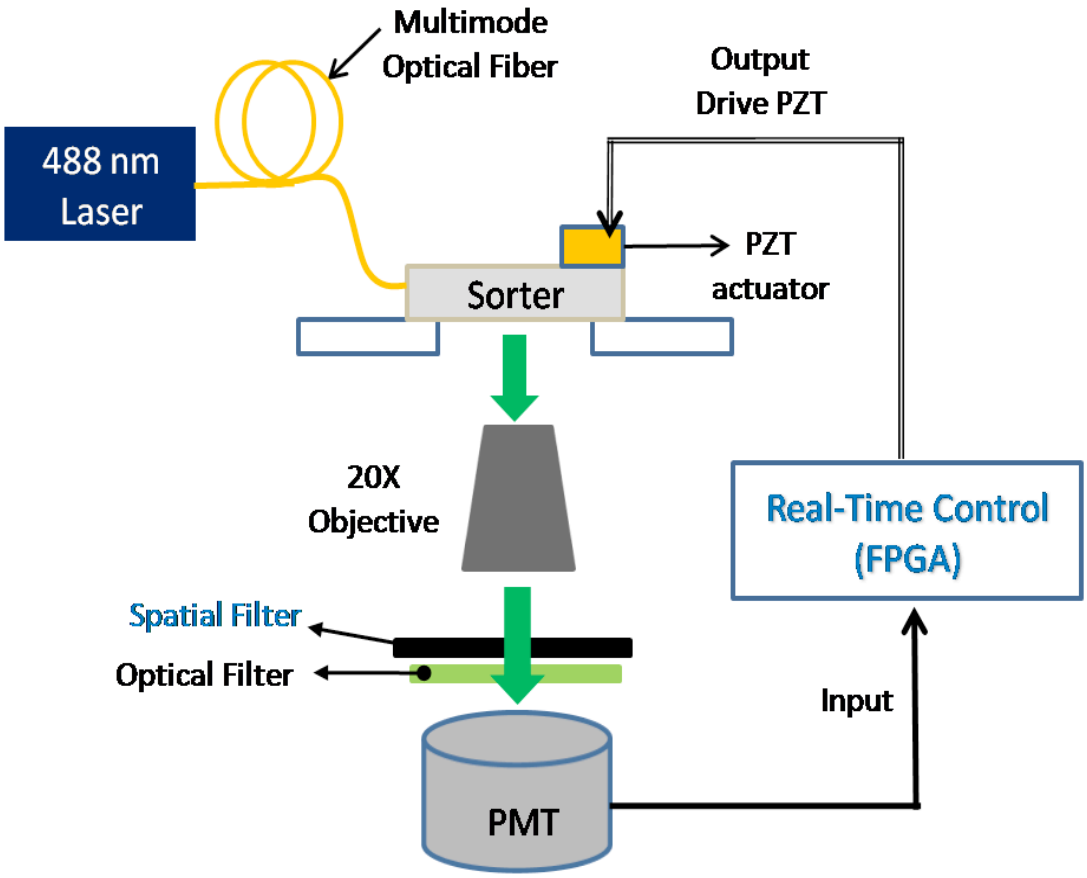

Figure 4.4 Schematic of the optical detection and control/sorting system setup. Specially designed spatial filters (masks) are placed at the image plane to modulate incoming fluorescence signals before those signals are registered by the PMT.

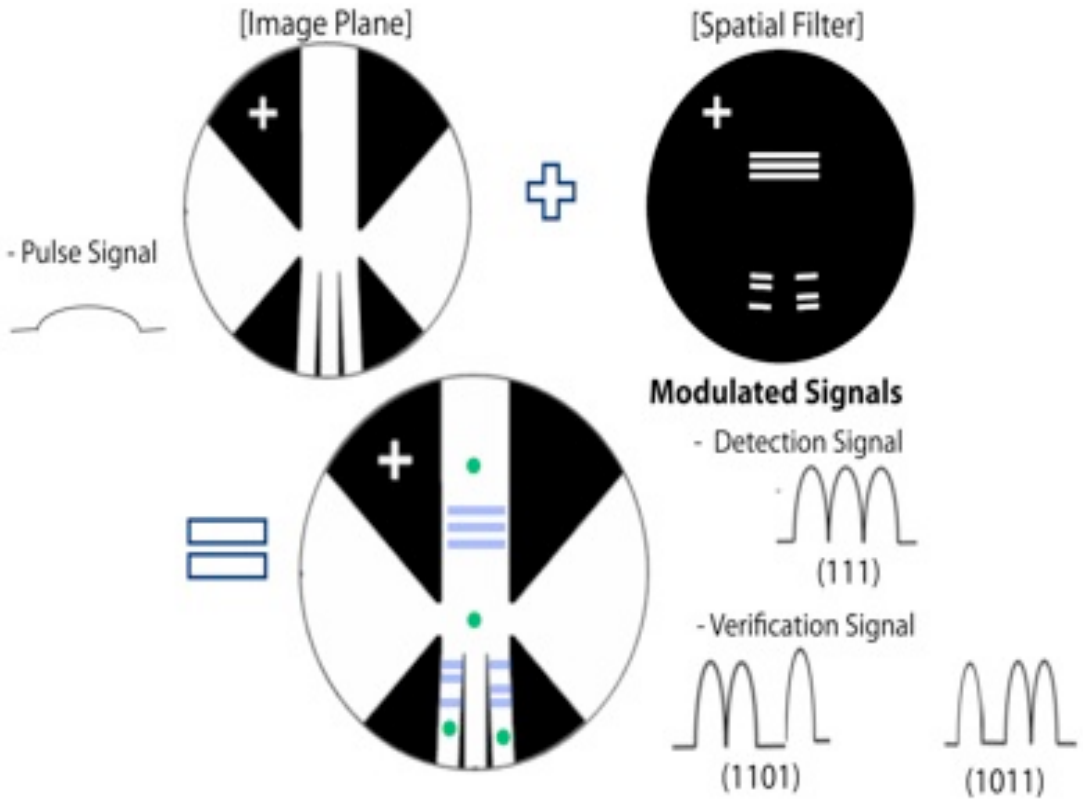

Figure 4.5 Spatial filters (masks) are specially designed and placed at the magnified image of the device feature. The input fluorescence pulse signal from stained cells is modulated by different spatial filters before being registered by the PMT, yielding different waveforms of photocurrents in time domain, corresponding to different locations of the cells as they travel through the microfluidics channel, such as (111), (1101) or (1011). This space-time coding technology reduces the size and the cost of the system by using only one PMT to differentiate three signals or even more.

In this manner, we have transformed the slit patterns on the mask into a time-domain signal of similar waveform, the space-time coding technique. As illustrated in Figure 4.5, different branches of the channels may have different slit patterns, resulting in different digital waveforms of the fluorescent signals detected by the same PMT. Using the space-time coding technique, we can keep track of the travel path of each cell (bead), a unique and very important feature for cell sorting without adding the size or cost of the signal. The output signal from the PMT is imported into the electronic control system for real-time processing. The control system is programmed with an external driver (CompactRIO, National Instruments Inc. USA) that has an embedded field programmable gate array (FPGA) chip.

The patterned slits are used to (1) code signals from the upstream detection zone and the downstream verification zone and (2) to temporally encode the signals so digital signal processing can enhance the signal-to-noise ratio. Since the waveform of the signal is predetermined by the slit patterns on the mask, digital matched filters can be applied to amplify the signal and suppress the noise. The signal processing algorithm can be implemented with finite-impulse-response (FIR) filters in real time.

In our system, the slits downstream from the sorting junction are designed to produce a digital pattern of (1011), distinguished from the (111) pattern in the detection area upstream of the sorting junction. After each cell is deflected to one of the sorting channels, the 'verification' signal (1011) should be detected to confirm the success of the sorting event. This single source, multi-point detection is possible because the excitation light is guided along the optofluidic waveguide even after the channel is split,

thus fluorescence will still be excited and detected after the cells are sorted. The verification signal can be exploited to calibrate sorting parameters, such as the magnitude of the voltage applied to the PZT actuator, or necessary time delay to actuate the PZT actuator for accurate sorting.

Real-time signal processing flow is illustrated in Figure 4. 6. First, spike noise from the PMT due to the thermoelectric effect (i.e. dark current) and cosmic rays are removed. Signals are selectively amplified based on the finite impulse response (FIR) filtering algorithm to amplify only the signals that have the same frequency spectrum as the spectrum of the designed FIR filter, while noise of different frequencies is suppressed.

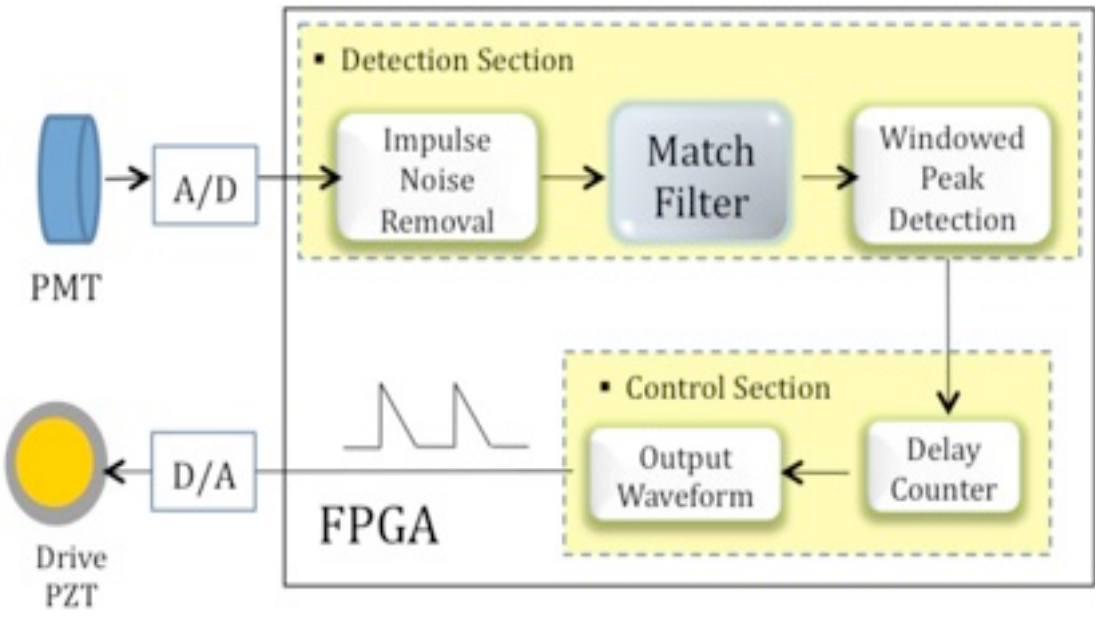

Figure 4.6 The FPGA implemented real-time process control unit consists of two sub-sections: the detection section and the control section. The timing jitter of the system is less than 10 μs, enabling the real-time control. The match filter is a critical component that enhances the signal to noise ratio significantly.

Figure 4. 7 shows the amplified signal with the FIR match filter algorithm. The FIR filter can enhance the signal-to-noise ratio (SNR) by 18 dB in real time, thus improving sensitivity and detection efficiency significantly. Any input signal above a user-defined threshold value implies the presence of a cell targeted for sorting. A delay counter in the control section can specify the elapsed time for the cell of interest to travel from the detection region to the sorting junction, and a pre-defined voltage signal

is employed to drive the PZT actuator at the correct time to deflect the cell into the sorting channel. The timing jitter is measured to be less than 10 μm. The timing jitter is significantly shorter than the travel time of the cell from the upstream detection spot to the sorting junction, minimizing the chance of a false sorting.

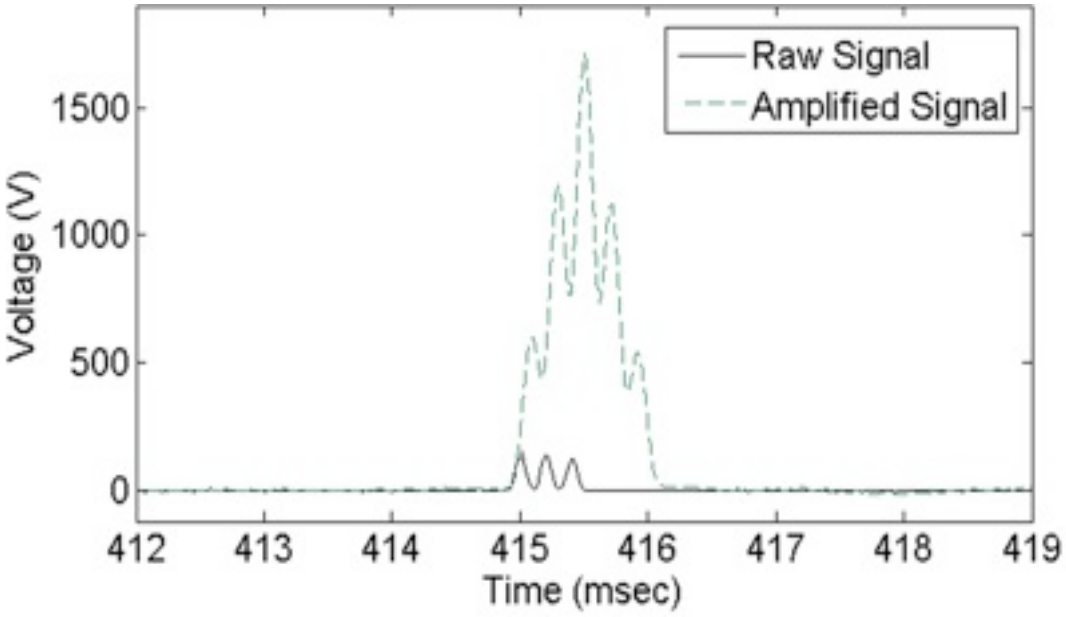

Figure 4.7 Comparison of the (111) coded raw signal with three small peaks with the amplified signal by applying the FIR match filter algorithm. The signal to noise ratio is enhanced by at least 18dB by the space-time coding technology. The enhanced detection sensitivity enables the μFACS to screen and sort out more cells of interest. There is also plenty room to set the threshold voltage to trigger the PZT actuator for sorting, thus reducing the possibility of 'false-sorting' due to the intensity fluctuation in detected fluorescent signals.

4. 6. Sample preparation

To characterize the performance of the integrated μFACS, 10 μm fluorescent polystyrene beads (Bangs Laboratory Inc., USA) are mixed with non-fluorescent 5 μm beads at an initial mixture ratio of 0.0067 (as determined by a commercial FACS machine FACScan; BD, USA) and a concentration of 1×10^7 beads / ml.

To validate the sorting capability for biological applications, a mixture of stained and non-stained K562 cells (human erythroleukemic cell line) was used. The fluorescent cells were prepared by incubation in 2 μM carboxyfluorescein diacetate succinimidyl ester (CFSE) in PBS/BSA at 37 ^{o}C for another 15 min. Following a second washing step, the stained cells are mixed with non-stained cells at an initial mixture of 0.0081 (determined by the commercial FACS) and a concentration of ~ 1.1×10^7 cells / ml. Before introduction to the μFACS device, the cells are filtered through a 40-μm cell strainer (BD Bioscience, USA) to remove large cell clumps. FACS fluid (BD Bioscience, USA) was used as sheath fluid for both aforementioned samples.

4. 7. Sorting purity analysis

Once the sorted mixture is collected, it is immediately transferred to a commercial FACS (FACScan, BD Biosciences) for purity analysis. To determine proper gating, a portion of the initial mixture is analyzed prior to sorted mixture. Gating by forward scattering (FSC) signals is used to determine total sample population. With the same gating, fluorescein histograms (FITC) of both the initial and the sorted

mixtures are analyzed to determine the respective mixture ratios and, therefore, the enrichment factor.

4. 8. Results and discussion

4. 8. 1. Separation of two different microspheres

A mixture of 10 μm fluorescent beads and 5 μm non-fluorescent beads with an initial mixture ratio of 1:160 is introduced to the μFACS device with sample flow and sheath flow rates of 5 mL min^{-1} and 50 mL min^{-1}, respectively. This flow generates an average bead velocity of around 5 cm/sec characterized using a high-speed camera. Utilizing the aforementioned space-time coding technique, sorting parameters to drive the PZT actuator can be optimized in the first few minutes of experiment, resulting in significant savings in sample volume.

As shown in Figure 4. 5, the modulated detection signal has a three-lobed waveform, and one can estimate the velocity of each cell from the time interval between the lobes and the shape of the lobe by deconvolving the waveform from the shape of the slits. For example, in Figure 4. 8, the estimated cell speed is 6 cm/sec, and the timing to trigger the PZT is determined based on the estimated velocity. The optimization process would result in the appearance of sorting signals (e.g. 1011 modulation) after detection signal (e.g. 111 modulation), as this indicates that targeted particles are being detected and sorted successfully. The intensity of the verification signal is lower than that of the detection signal because the excitation light intensity has been divided into three branches, and the (1011) slit design has a slightly different spatial frequency. The

intensity fluctuation observed in the verification signal is due to the loss of flow confinement, as the 2-D flow focusing is broken after the sorting junction.

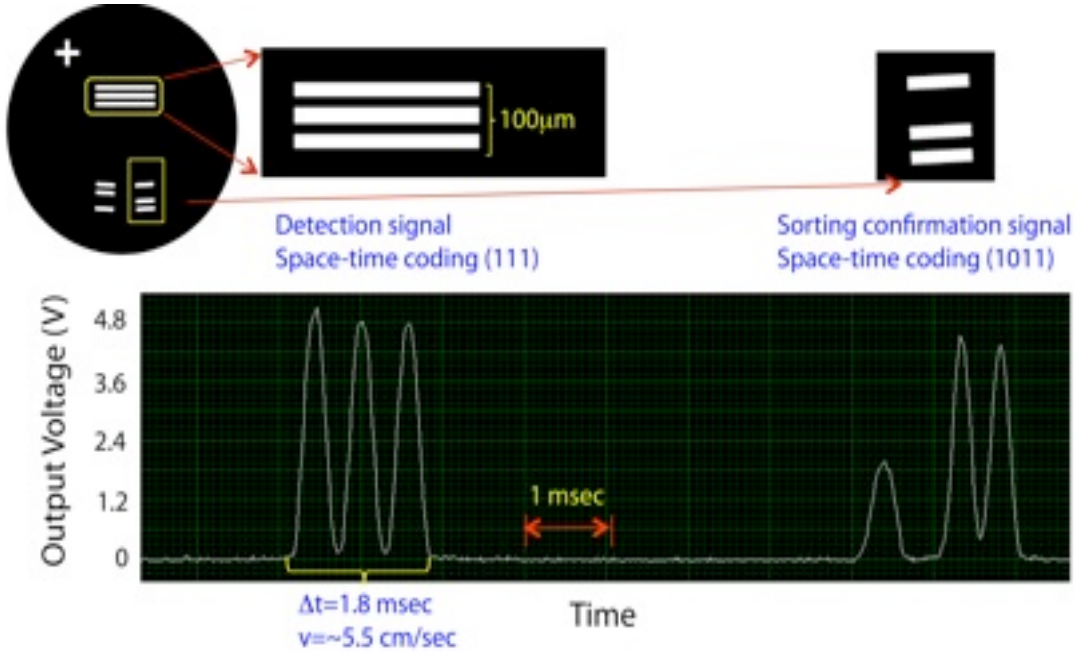

Figure 4.8 Example of space-time coding signals out of 10 μm fluorescent polystyrene beads. The first signal coded as (111) represents the detected fluorescence when the bead passes the detection zone (e.g. three transparent slits). After sorting, the second signal coded as (1011) that is ~ 5msec trailing the detection signal indicates that the bead has been correctly switched into the sorting channel, confirming the successful sorting event. Note that the first signal allows one to estimate the velocity of the bead roughly, helping determine the right delay time for the exact triggering of the PZT actuator. Here, the bead travels with a velocity of around 5.5 cm/sec.

After continuous automated sorting for ~ 30 min with the optimized sorting parameters, the sorting result shows a ~ 200 fold enrichment at a throughput of 1500 beads/sec. The results, shown in Figure 4. 9 and in Figure 4. 10 are very consistent from run to run are very consistent under the same flow conditions and sample preparation. The output mixture ratio between the 10 μm fluorescent beads and the 5 μm non-fluorescent beads is about 1.3: 1 after sorting while the initial ratio is 1: 160. The output mixture ratio implies that some unwanted 5 μm beads are sorted accidentally even though the 10 μm beads are significantly purified. This occurs because the velocity of the beads is not constant due to the lack of 3D (vertical direction) flow confinement. This causes an error in defining the proper timing for triggering the actuator, occasionally deflecting the unwanted beads into the target channel. Given the velocity of the beads (5 – 7 cm/sec) and the initial concentration (~ 10^7 beads/ml), the average distance between two beads is about 50 – 80 μm, which implies the possibility of accidentally sorting two cells in one actuation since the nozzle opening at the sorting junction is 100 μm wide.

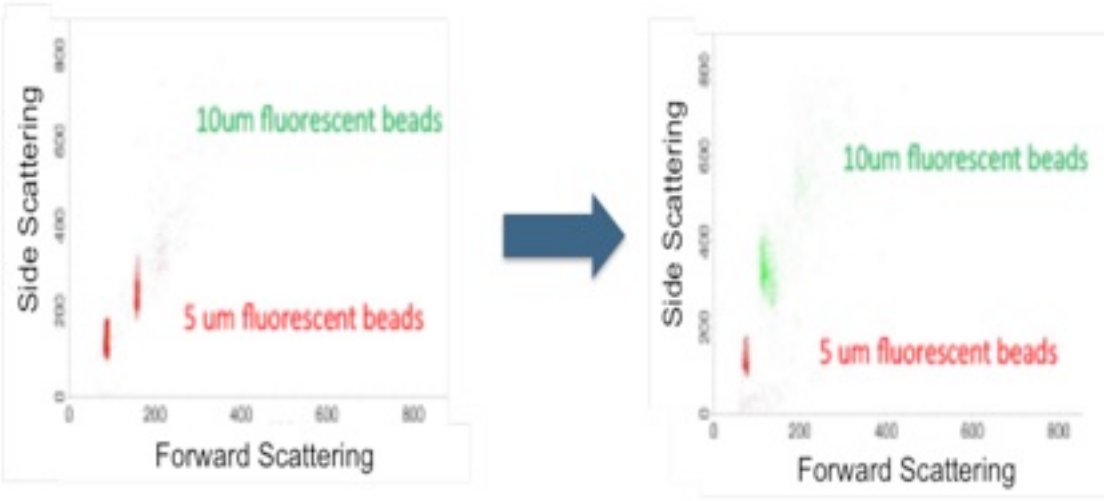

Figure 4.9 The scattering plots show the result of sorting fluorescent 10 μm beads from non-fluorescent 5 μm beads. After sorting (Right), the population of the green fluorescent beads has been enriched by a factor of about 200 fold.

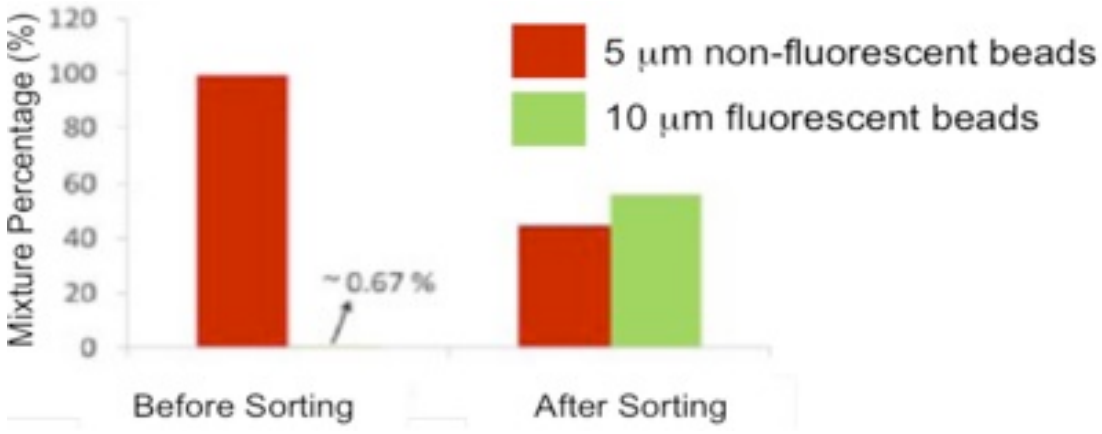

Figure 4.10 The population ratio of the initial bead mixture is 0.67: 100. After sorting for 30 min, the mixed ratio becomes 1.3: 1, yielding an enrichment factor of around 200.

4. 8. 2. Sorting biological samples – Human mammalian cell and E. Coli

Feasibility of the integrated micro-sorter for biological application is demonstrated using human erythroleukemic (K562) cells and E.Colis. Under similar flow conditions, sample concentration, and initial mixture ratios, flow cytometric analysis shows an enrichment factor of ~ 230 fold as shown in Figure 4. 11, which is the highest value ever demonstrated in μFACS systems. Based on the sample flow rate (6 μl / min) and the cell concentration (1.1×10^7 cells/ml), a throughput of ~ 1000 cells/sec is achieved. Even though the sample concentration is relatively high compared to conventional flow cytometric analysis (~ $10^6 – 10^7$ cells/ml), no significant cell stiction is observed due to the chemically inert Teflon AF coating. Cell clogging, which is common among μFACS systems, can greatly compromise sorting purity as well as the ability to collect sufficient targeted cells because the device becomes unusable as the clogged cells block the fluid flow. Owing to its minimized clogging, the proposed system can sustain continuous operation for long periods of time (> 2 hours). This is essential for sorting of rare cells such as stem cells and circulating tumor cells.

Fluorescently labeled E.colis are also sorted using the same μFACS device, and the sorting result is shown in Figure 4.12. The microfluidic FACS works well and gives consistent sorting results (e.g. enrichment factor around 200 fold) regardless of the physical or chemical properties of the samples being sorted. This is attractive as one single device structure can sort a variety of biological samples, while most of other microfluidic-based sorting mechanisms rely on physical or chemical properties such as shape, density, dielectric property, size etc[1, 2, 4-6].

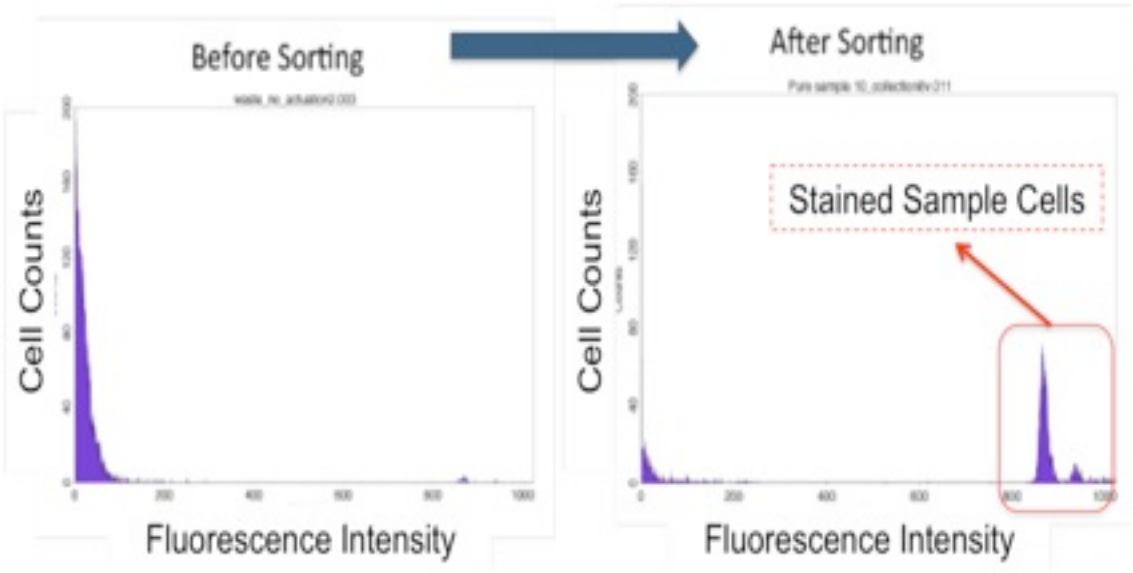

Figure 4.11 Before sorting (Left), most of cells are non-fluorescent (e.g. showing very low fluorescent intensities) as the mixed ratio of fluorescent cells to non-fluorescent cells is 1: 150. After sorting, the histogram (Right) shows that the population of the sample (e.g. fluorescent cells) is purified with an enrichment factor of 230. The red dotted box shows the purified sample population after being sorted. The sorting experiment ran more than 2 hours without significant cell stiction to the wall or clogging the channel because the Teflon AF coating layer is chemically stable and inert.

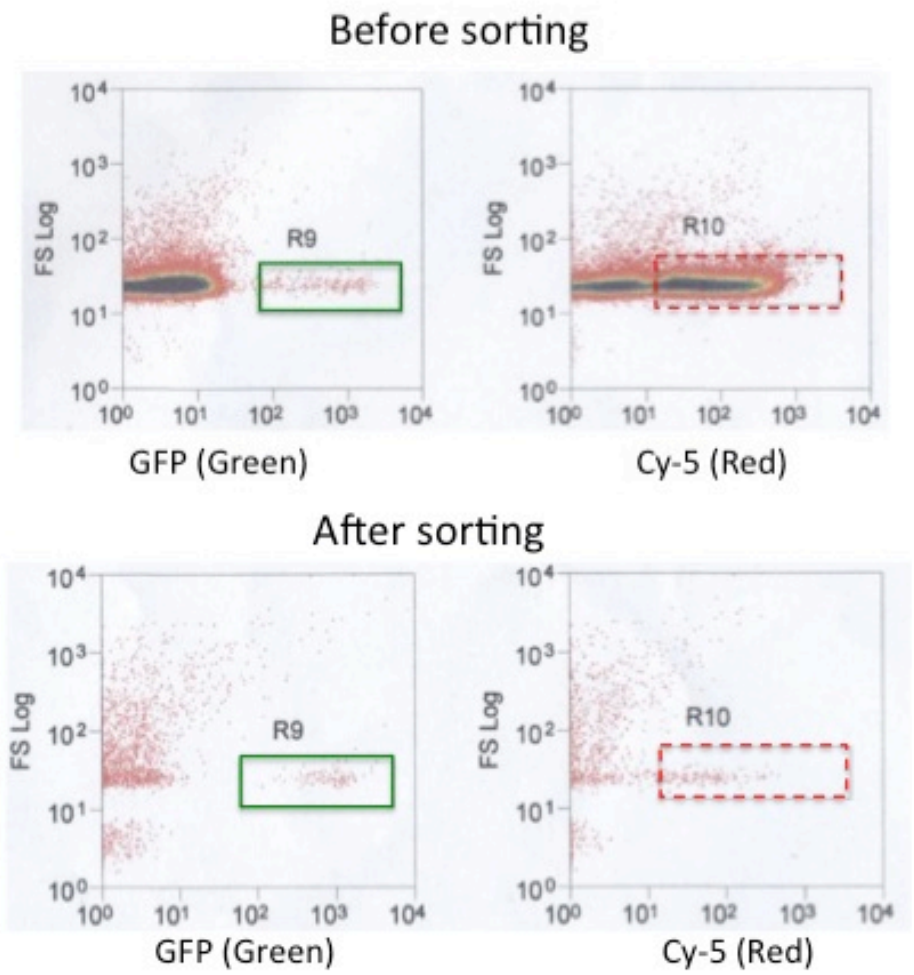

Figure 4.12 Fluorescently labeled E.colis samples stained by fluorescence in situ hybridization (FISH) are sorted using the same μFACS device as used for sorting polystyrene beads and human mammalian cells. The initial mixed ratio of the green stained E.colis (e.g. samples) to red stained E.colis is 1: 280. After sorting, however, the mixed ratio is about 0.8: 1, which means the sample E.coli population has been purified with an enrichment factor of 225 fold.

In conventional FACS, loss of cell viability is a concern due to the high hydrodynamic forces involved in the acceleration, droplet formation, and the deceleration as cells enter the collection tubes, etc [7]. A trypan blue exclusion test was performed to evaluate viability for unsorted cells and sorted cells by the PZT actuation. No significant loss of cell viability due the PZT actuation relative to unsorted populations was observed (less than 3%), which proves the PZT actuation mechanism does not cause serious damage to cells as sorted cells are deflected with the fluid.

In spite of the encouraging sorting capabilities of the μFACS, there are still two main challenges to be overcome: reducing the "tail-gating" and "catching-up" errors. From the sorting results for polystyrene beads, mammalian cells and E.colis, it is shown that over a wide range of ratio of initial mixture, the ratio of population after sorting is close to ~1:1, which implies that the population of sorted sample and the population of samples sorted by mistake are comparable.

This finding implies that the dominant error mechanism for sorting is "tail-gating" error. As the targeted cell is sorted by the actuator, it is likely that the cell trailing the targeted cell is also sorted due to the disturbance caused by the rapid flow switch. Another dominant error mechanism is the lack of three-dimensional flow confinement. Depending on the position of the cell in z-direction, the targeted cell identified at the optical interrogation zone can potentially be caught by an untargeted cell that travels at a higher speed so that both cells may arrive the sorting zone at the same time. As a result, both the targeted cell and the untargeted cell are sorted together, thus limiting the enrichment factor.

4. 8. 3. Comparison to commercial FACS

To compare the sorting performance of the integrated μFACS with one of the highest performance bench-top FACS, (MoFlo; DakoCytomation Inc., San Diego, CA), nearly identical experimental conditions (sample concentration, initial mixed ratio, and throughput) are intentionally utilized using the bead sample (i.e. mixture of 10 μm fluorescent and 5 μm non-fluorescent beads). The result is down in Table 4. 1. While the MoFlo outperforms the integrated μFACS in terms of sample enriching capability, the gap is not too large considering the sophistication, size, and price (~$500K) of the MoFlo system.

The μFACS system could significantly bridge this gap in sample enrichment by incorporating the capabilities of scattering parameter measurement, three-dimensional flow confinement, and the use of a narrower nozzle structure. Since the current system performs sorting based only on fluorescence detection, the addition of a scattering parameter can enhance purity by aborting sorting decision whenever cells are traveling too close together.

With 3-D flow confinement and a narrower nozzle structure, the effect of velocity variation in the vertical direction can be minimized, further preventing two beads from being sorted together due to the close distance between them. For future work, incorporation of the FSC parameter can be achieved by integrating on-chip waveguide-lens structure that allows in-plane optical excitation and collection [8, 9]. A number of 3-D flow confinement architectures, such as those employing the microfluidic drifting technique [10] or chevron structures [11] or else are compatible with the

current system and can be readily integrated with the new device structure for increasing purity while maintaining high throughput operation.

Table 4.1 Comparison to the commercial FACS, MoFlo

Instrument	Throughput	Initial Mixture Ratio	Final Mixture Ratio	Enrichment
Integrated μFACS (Beads)	1500 (beads s^{-1})	0.0067	1.34	200 fold
Integrated μFACS (Mammalian Cells)	1000 (cells s^{-1})	0.0081	1.86	230 fold
MoFlo (Beads)	2000 (beads s^{-1})	0.0098	9.02	920 fold

4. 8. 4. Cost and size reduction

Low cost and portability are desirable features of microfluidics-based FACS. The μFACS device presented in this paper shows potential for significant (10 to 100 times) cost and size reduction while producing good performance. The on-chip PZT actuator and PDMS monolithic structure contribute to the dramatic size and cost reduction and enhanced functionality. The lost sensitivity due to the limit of on-chip optics compared to the bulk optics in bench top systems can be more than compensated by the space-time coding technique elucidated in this paper. All these make the lab-on-a-chip μFACS system attractive to point-of-care clinics and diagnostics in developing countries.

4. 9. Conclusion

In this chapter, we have demonstrated a lab-on-a-chip cell sorter with an integrated piezoelectric actuator and fluidic optical waveguide to achieve high sensitivity and multi-point detection. As excitation always occurs, fluorescence can be detected at multiple points. A real-time signal processing and control system to allow closed-loop sorting is implemented in FPGA. The device operates under low power (less than 1mW) and allows for a high throughput (~ 1500 cells/sec) as the flow stream responds to the piezoelectric actuator at high frequency. These attractive and unique features hold promise for a high-performance, low cost, and portable lab-on-a-chip μFACS system.

Sorting by this method does not depend on any properties of cells, as it operates by manipulating small volumes of fluid containing cells, thus allowing any kind of biological samples to be sorted and purified. The Teflon AF coating layer allows the sorting of biological samples by eliminating the issue of cell stiction and permeation through PDMS that many other μFACS systems suffer from. This system's ability to manipulate single particles also allows one to sort samples at a high throughput and to achieve high purity. In fact, if a cascade structure is implemented for the 2^{nd} round of sorting, enrichment of up to ~ 1M-fold or even higher should be possible.

References:

1. H. Bang, C. Chung, J. Kim, S. Kim, S. Chung, J. Park, W. Lee, H. Yun, J. Lee and K. Cho, Microsystem Technologies **12** (8), 746-753 (2006).

2. A. Wolff, I. Perch-Nielsen, U. Larsen, P. Friis, G. Goranovic, C. Poulsen, J. Kutter and P. Telleman, Lab on a Chip **3** (1), 22-27 (2003).

3. S. Cho, J. Godin and Y. Lo, IEEE Photonics Technology Letters **21** (15), 1057 (2009).

4. N. Pamme and C. Wilhelm, Lab on a Chip **6** (8), 974-980 (2006).

5. J. Voldman, M. Gray, M. Toner and M. Schmidt, Anal. Chem **74** (16), 3984-3990 (2002).

6. M. Wang, E. Tu, D. Raymond, J. Yang, H. Zhang, N. Hagen, B. Dees, E. Mercer, A. Forster and I. Kariv, Nature biotechnology **23** (1), 83-87 (2004).

7. J. Seidl, R. Knuechel and L. Kunz-Schughart, Cytometry Part A **36** (2), 102-111 (1999).

8. J. Godin, V. Lien and Y. Lo, Applied Physics Letters **89**, 061106 (2006).

9. V. Lien, Y. Berdichevsky and Y. Lo, IEEE Photonics Technology Letters **16** (6), 1525-1527 (2004).

10. X. Mao, S. Lin, C. Dong and T. Huang, Lab on a Chip **9** (11), 1583-1589 (2009).

11. J. Golden, J. Kim, J. Erickson, L. Hilliard, P. Howell, G. Anderson, M. Nasir and F. Ligler, Lab on a Chip **9** (13), 1942 (2009).

Chapter 4 or portion thereof has been published in *Lab on a Chip*, Sung Hwan Cho, Chun-Hao Chen, Frank S. Tsai, Jessica M. Godin, and Yu-Hwa Lo, vol. 10, 1567 (2010)

Chapter 5

Lab-on-a-chip multi-color flow cytometer employing color-space-time (COST) coding

In this chapter, we will present a novel way of fluorescent detection for a lab-on-a-chip multicolor flow cytometer. Fluorescent emission spectrum is encoded into a time-dependent signal as a fluorescent cell or biological sample traverses a waveguide array with integrated spatial filters and color filters. Different from conventional

colored filters with well-defined and sharp transmission spectral window, the integrated color filters are designed to have broad transmission characteristics, similar to the red-green-blue photoreceptors in the retina of human eye. This technique called "color-space-time (COST)" coding allows us to detect multiple fluorescent colors with only three on-chip color filter waveguides using only one single photomultiplier tube or avalanche photodetector resulting in significant reduction in the size and the cost of the off-chip detection system.

5. 1. Introduction

Flow cytometers incorporate fluorescent detection for a greater ability to obtain detailed identification of cell types and functions based on fluorescence of antibody-conjugated dye labels. The most advanced systems can measure as many as seventeen fluorescent colors. Such multicolor detection system find various applications in immunophenotyping and stem cell research since multi-color staining on samples of interest enables for more specific sub-categorization [1-3].

In spite of the valuable information of obtained from the multicolor flow cytometers, the detection of multiple fluorescent colors requires many dichroic mirrors, interferometric filters and photomultiplier tubes (PMTs) in order to isolate the spectral region of interest. This is the key reason why today's bench top flow cytometers are still bulky, costly, and not easy to operate, thus having only limited use for point-of-care applications.

Lab-on-a-chip platform flow cytometers, on the other hand, are promising for point-of-care applications because they are potentially much cheaper and easier to use than commercially available bench-top systems. However, although most microfluidic flow cytometer systems integrate fluidic parts and, to a very limited extent, some optical components on a single chip, they still need expensive and bulky peripheral optic and detection devices such as multiple dichroic filters and PMTs for fluorescent light detection. Concerning flow cytometers, the lab-on-a-chip approach is not attractive unless there is a significant reduction in cost and size of the whole system, which means the bulk optics and, in particular, the number of PMTs are reduced significantly.

Since all current flow cytometers, being bench-top systems or lab-on-a-chip systems, require one dedicated PMT for detection of each fluorescence color, it calls for an innovative architecture, besides device technologies, to fundamentally alter the scaling rule (i.e. the number of optical components and PMTs does not linearly scale with the number of detection parameters). We tried to come up with a novel way to solve this big problem, and we realized that the solution lies in human eyes that can distinguish more than 1,000 different colors using only three types of photoreceptors.

5. 2. Color-Space-Time (COST) coding technique mimicking human eyes

To solve the above problem of reducing cost and size of the detection system, we invented a novel and innovative fluorescent color detection method, which is called color-space-time (COST) coding, for lab-on-a-chip multicolor flow cytometer applications. This new technique is an expansion of the “space-time” coding technique

mentioned in the previous chapter (Chapter 4), that converts the spatial information into time domain signals, thus enabling for sharing one laser for multi-spot excitation and detection[4-7].

The COST coding encodes a fluorescence emission signal into a time-dependent signal when each fluorescent object passes by an array of on-chip transverse spatial filters and color filter waveguides. The on-chip spatial filters in the form of an array of apertures are made of black polydimethylsiloxane (PDMS) (Sylgard 170, Dow Corning). These spatial filters produce a specific signal waveform in time domain as illustrated schematically in Fig. 5. 1.

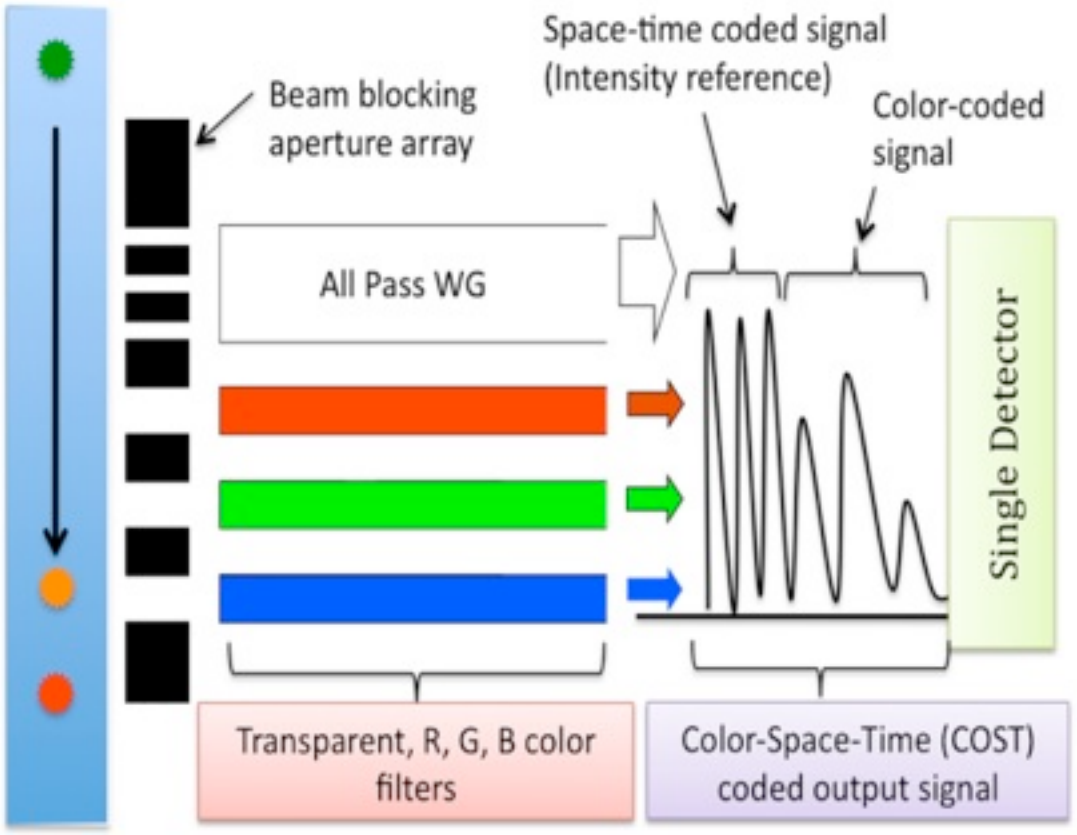

Figure 5.1 Schematic illustration of COST coding design. Each fluorescent color is first space-time coded by the first transparent waveguide, and then, color-coded by the red, green, and blue color filter waveguide array. The COST coded signal is registered by one single PMT instead of using multiple PMTs.

In order to add fluorescent color signals into the waveform, three waveguides each filled up with color-specific light absorption material are introduced so that the intensity of the last three peaks of the signal contain information about the fluorescent color. To separate color information from the overall fluorescence intensity of each

fluorescent particle, the three leading peaks of the signal are produced from an all-pass waveguide and used as the reference intensity for each fluorescent particle. Therefore, wide distribution in fluorescent signal intensities is taken care of automatically. A single detector (i.e. PMT) then registers the COST-coded signal, as illustrated in Figure 5.1.

5. 3. Fabricating on chip color filter waveguides and COST device

A COST device that provides multicolor detection on a lab-on-a-chip platform is fabricated using PDMS and glycerol. Glycerol is a good material for the waveguide core because it is optically transparent and has a higher refractive index (n=1.47) than that of PDMS (n=1.41) as the waveguide cladding material. We inject oil-soluble color dyes mixed with high refractive index glycerol into the core of on-chip waveguides as color filters to code each fluorescent color. It has been demonstrated that color dyes mixed with glycerol do not diffuse into the PDMS cladding layers, thus resulting in stable color filter waveguides [8].

Orange food color powders (AmeriColor Co.), phthalocyanine blue dyes (TCI Chemicals, Inc.) and blue food color powders (AmeriColor Co.) are chosen to form the red, green, and blue color filter waveguides, respectively. After calibrating the concentration of each color filter in glycerol, we achieve the desired transmission spectrum of each waveguide filter as shown in Figure 5.2. Figure 5.3 shows dye-doped glycerols.

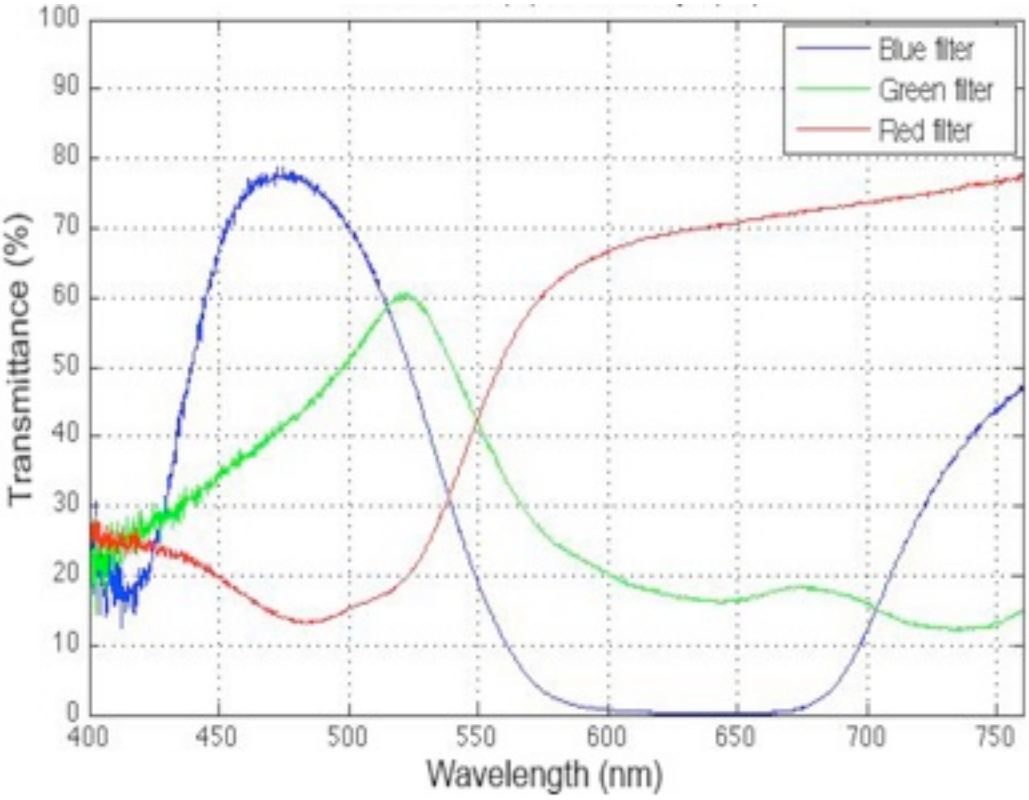

Figure 5.2 Transmission characteristics (from 400 nm to 750 nm) of red, green, blue color filters. Each waveguide is 1 cm long. Broad transmittance spectrum filters with different peaks allow multicolor discrimination analogous to the human eye. Red filter: food color orange (300 μg/ml), Green filter: phthalocyanine blue (200 μg/ml), and Blue filter: food color blue (600 μg/ml)

Figure 5.3 Dye doped glycerols.

The microfluidic COST device is fabricated by PDMS replica molding process using an SU-8 mold formed photolithographically on a silicon wafer. The device contains several structures including (i) microfluidic channels, (ii) apertures and color filter waveguides, and (iii) another channel structure for filling the apertures and the waveguide channels. Patterns in [(i) and (ii)] and in (iii) are formed on two separate PDMS substrates first and then the two PDMS substrates are UV/Ozone bonded together permanently with an alignment accuracy better than 10 μm by using a stereoscope.

Figure 5.4 (a) shows the layout of the device consisting of two (black and red) layers of patterned PDMS that are permanently bonded together. The black patterns in

Figure 5.4 (a) are the main channels carrying biological samples, the apertures blocking stray light, and the color filter waveguides. The red patterns are channels for fluids filling to create the apertures and the color filter waveguides. Figure 5.4 (b) shows the side view of the device across lines (1) and (2) of Figure 5.4 (a). Figure 5.4 (c) shows well-aligned top and bottom PDMS layers. The apertures for space-time coding and for stray light blocking are filled with black PDMS by the capillary effect. After 30 min of curing, the all-pass (i.e. dye-free glycerol) and RGB color filter waveguide channels are filled with appropriately doped glycerol by the capillary effect as well. All the waveguides are filled without any air bubbles inside.

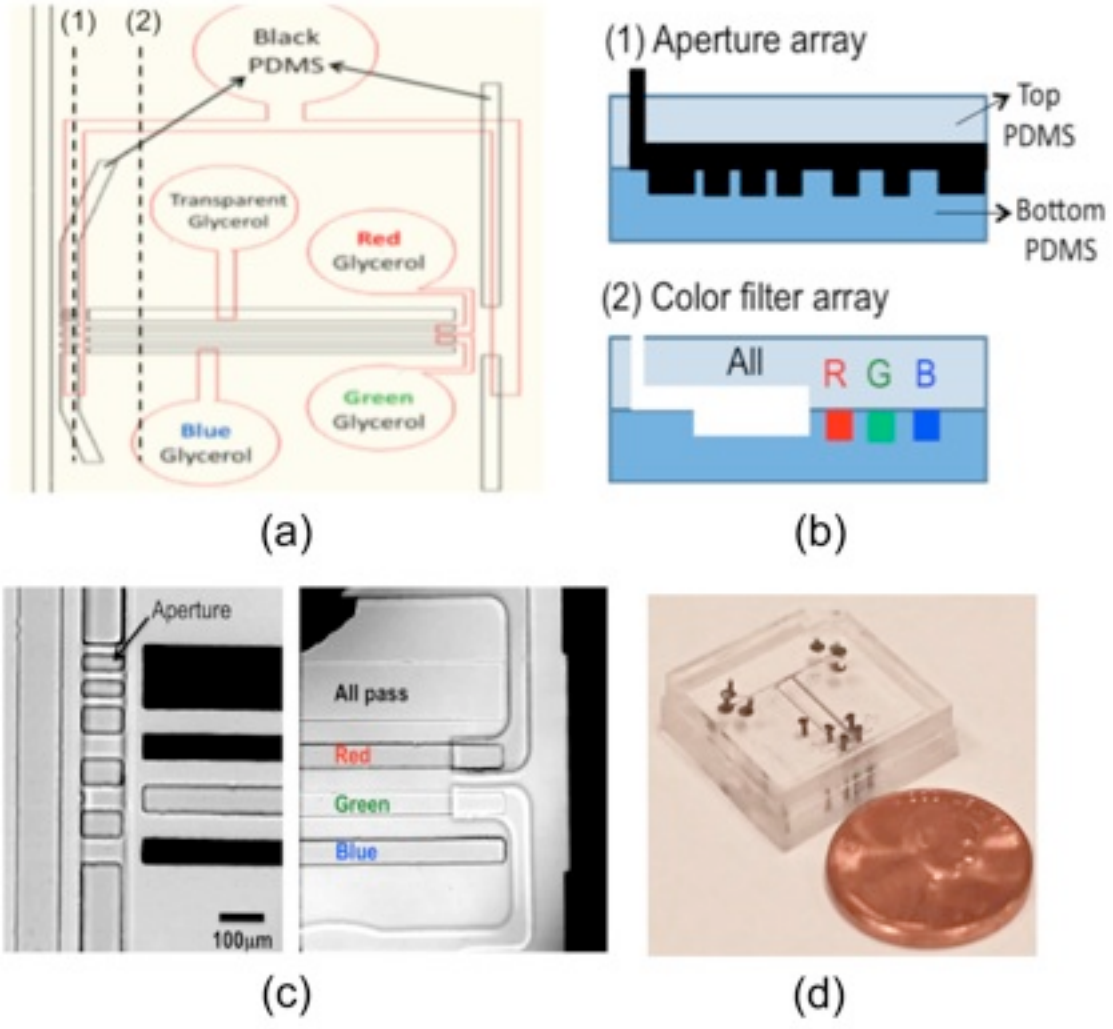

Figure 5.4 The layout of the microfluidic COST device. (a) The black patterns are for the main channels, the apertures, and the color filter waveguides. The red patterns are channels used for filling those apertures and color filter waveguides with appropriate polymers. (b) Side view of the device across lines (1) and (2) of Figure 5.4. (a). (c) The top and bottom PDMS layers are aligned and the waveguides and apertures are filled. (d) The picture of the completed COST device. It is as small as a penny.

5. 4. COST-coded color fingerprints

To distinguish as many fluorescent colors as possible, we have each color [red-green-blue (RGB)] waveguide show a gradual change in its transmission spectrum in a similar manner to the photoreceptors found in the combs of human retina [9]. The gradual, wideband color filtering reduces the required number of samples to differentiate multiple colors, and its principle has been manifested by our eye's ability to distinguish more than 1000 colors using only three kinds of photoreceptors. For lab-on-a-chip flow cytometers, we attempt to use three on-chip color-filtered waveguides to detect as many as 11 wavelengths using a single PMT only.

Using the microfluidic COST flow cytometer, we demonstrate that two fluorescent micro beads emitting two different, although similar, colors can be distinguished using a single PMT (PMM02, Thorlabs Inc.). The experimental setup is schematically illustrated in Figure 5.5. A 488nm wavelength diode laser (40mW, Coherent) is used as the source to excite the fluorescent beads in the microfluidic channel. The spot of the excitation laser has a Gaussian intensity profile, and the laser intensity across the 450 μm waveguide regime is calibrated using a charge-coupled device camera. In the final data analysis for color discrimination, the effect of laser intensity distribution is removed.

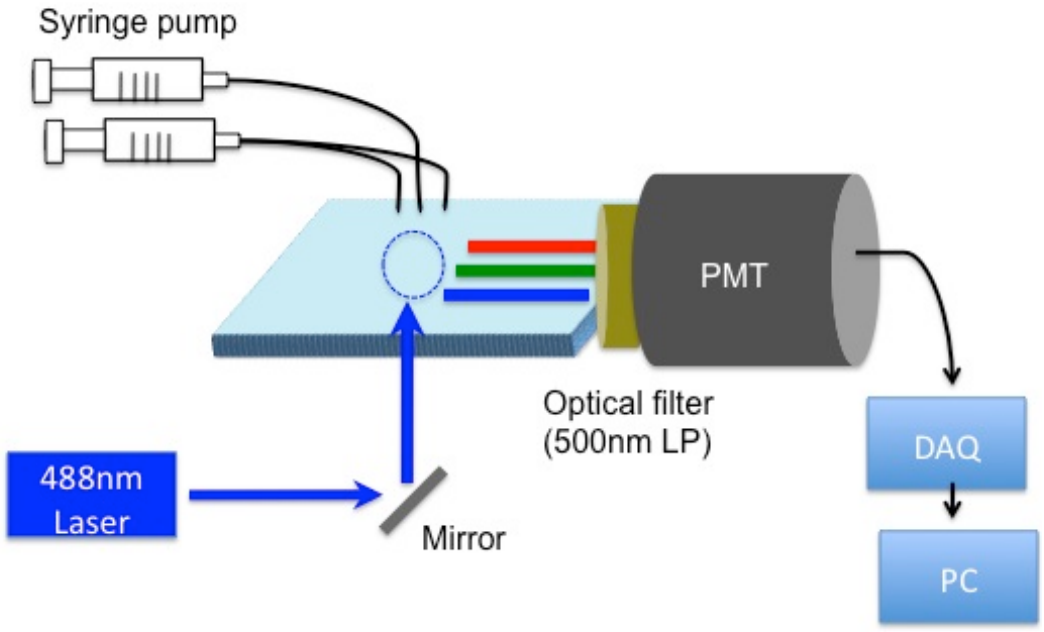

Figure 5.5 Experimental setup of the color-space-time (COST) system to distinguish dragon green and envy green fluorescent beads. A diode laser with 488 nm wavelength was used to excite fluorescent beads and an optical long pass filter with the cutoff wavelength of 500 nm was placed in front of the photomultiplier tube (PMT) to block the strong excitation light.

Figure 5.6 (a) shows a typical waveform of the COST coded output signal from a dragon green fluorescent bead. The emission peak is at 520 nm, equivalent to fluorescein isothiocyanate (FITC) fluorochrome that is widely used in flow cytometers. The first three identical peaks are space-time coded signals. They establish the reference for the overall fluorescence intensity so that the fluorescence intensity variations among different beads will not affect our ability to determine the fluorescent

colors. The following three peaks have different intensities, on the other hand, because each peak is produced by the corresponding color filter based on the overlap between the emission spectrum of each type of fluorophore and the transmission spectrum of the color filter.

In consequence, the intensity ratios among these three peaks produce a unique fingerprint for each type of fluorophore. Figure 5.6 (b) shows the histogram of the green filtered COST-coded signal of the dragon green and the envy green (emission peak at 565 nm) fluorescent colors, which is normalized to the red filtered signal. In the same way, the histogram of the blue-filtered COST-coded signal of the two fluorescent colors is shown in Figure 5.6 (c). Those histograms show clearly that two different colors are coded differently and separated enough to be distinguished by one PMT instead of using two PMTs.

Table 5.1 Dragon green and Envy green fluorescent colors are represented by two vectors [1.00:1.63:1.24] and [1.00:0.80:0.64], respectively

	COST coded color fingerprint		
	Red filter	Green filter	Blue filter
Dragon Green (emission at 525 nm)	1	Mean=1.63 STD=0.046	Mean=1.24 STD=0.055
Envy Green (emission at 565 nm)	1	Mean=0.80 STD=0.060	Mean=0.64 STD=0.034

As shown in Table 5.1, dragon green is represented by a vector [1.00, 1.163, 1.24], while envy green is represented by a vector [1.00, 0.80, 0.64]. The variations (e.g. standard deviation of each peak) for each "color fingerprint" are between 2% and 7%. The variation should be minimized in order to discriminate as many colors as possible, and the lack of three-dimensional flow confinement and the intrinsic electronic noise needs to be addressed.

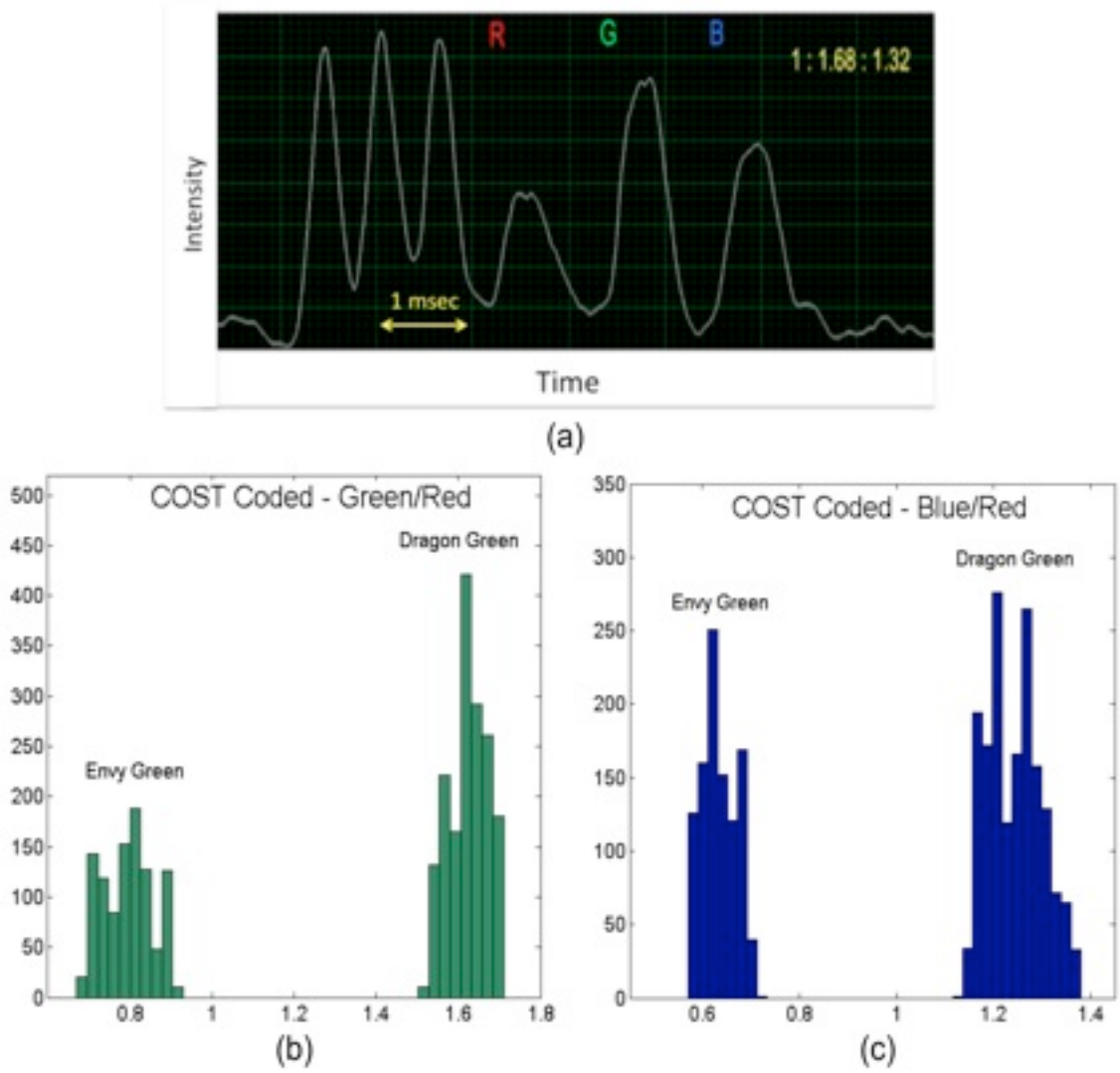

Figure 5.6 (a) COST modulated signal of Dragon Green fluorescence. The first three lobes are space-time coded signals, and the following three peaks are the COST coded signals. (b) Histogram of the green filtered COST-coded signal normalized to the red filtered signal intensity of Dragon Green and Envy Green. (c) Histogram of the blue filtered COST-coded signal of Dragon Green and Envy Green

Likewise, more fluorescent colors can be represented by their unique fingerprints according to the intensity ratios of (green/red, blue/red). The overlap between the emission spectrum of each fluorophore and the transmission spectrum of the RGB color filters in Figure 5.2 determines the center position of each fluorophore in Figure 5.7. The ellipse around each color represents the boundary of 5% fluctuation of the color ratio. From the data in Figure 5.7, we concluded that 11 different commonly used fluorophores in flow cytometers can be detected with a single PMT using the COST technique. Ultimately the number of colors that can be detected with the COST technology will be limited by the electronic noise and the lack of three dimensional flow focusing. These issues will be address in the near future.

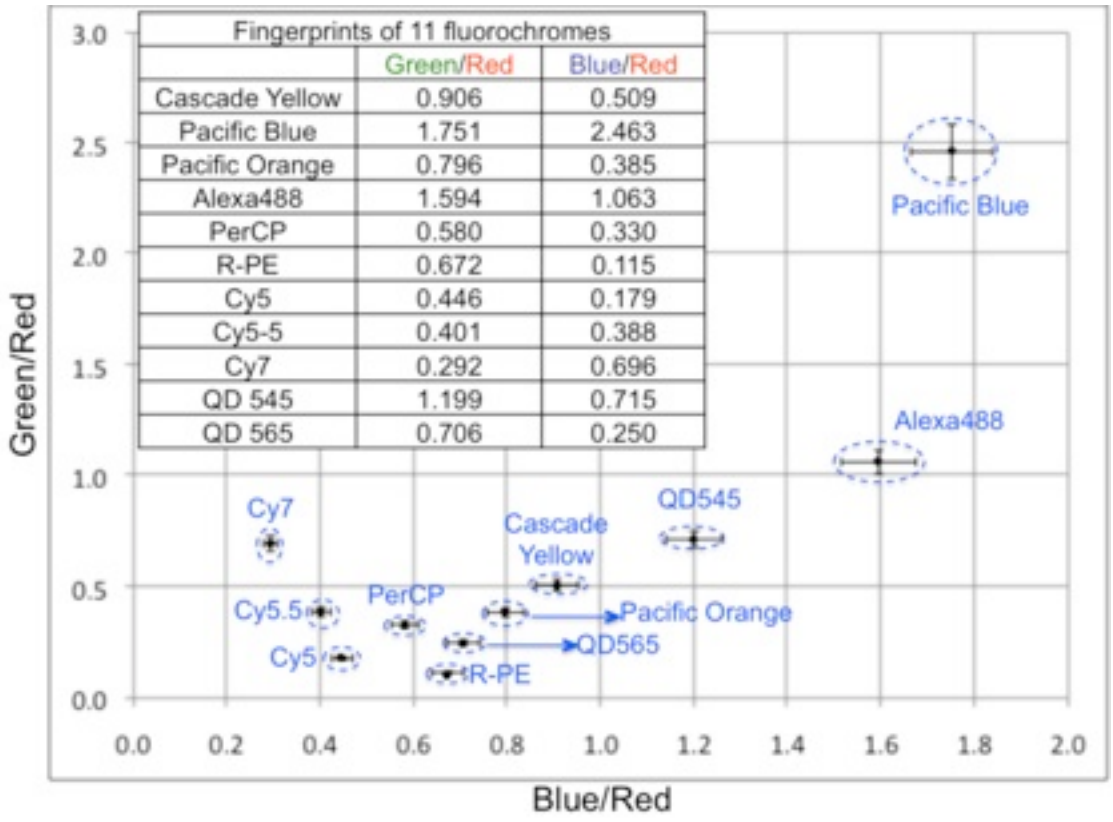

Figure 5.7 Each fluorescent color in the table has its fingerprint presented by the blue/red and green/red intensity ratios. The ellipse around each center position is the boundary of 5% fluctuation in the intensity ratios. The figure shows 11 different commonly used fluorophores in flow cytometers can be distinguished with a single PMT using the COST coding technique.

5. 5. Conclusion

In this chapter, we discussed a novel fluorescent detection method that can be applied to lab-on-a-chip flow cytometers for potential point-of-care applications. Using the COST technique, beads of two different fluorescent colors can be distinguished using a single PMT. The architecture is highly scalable and we have shown that as many as 11 commonly used fluorophores in flow cytometers can be potentially distinguished with a single PMT or APD.

Since bulky optics and a large number of PMTs are the bottleneck for the cost and size reduction in today's flow cytometers and the key reasons for system failures and high maintenance, the lab-on-a-chip technology in conjunction with the COST technique holds great promise for compact, cost effective, and easy to use flow cytometers for point-of-care applications.

References:

1. N. Baumgarth and M. Roederer, Journal of immunological methods **243** (1-2), 77-97 (2000).

2. P. Chattopadhyay, D. Price, T. Harper, M. Betts, J. Yu, E. Gostick, S. Perfetto, P. Goepfert, R. Koup and S. De Rosa, Nature medicine **12** (8), 972-977 (2006).

3. S. De Rosa, L. Herzenberg and M. Roederer, Nature medicine **7** (2), 245-248 (2001).

4. C. H. Chen, S. H. Cho, F. Tsai, A. Erten and Y.-H. Lo, Biomedical microdevices (2009).

5. S. H. Cho, C. H. Chen, F. S. Tsai, J. Godin and Y.-H. Lo, Lasers and Electro-Optics (CLEO) and Quantum Electronics and Laser Science Conference (QELS), 2010 Conference on, 1 - 2 (2010).

6. S. H. Cho, C. H. Chen, F. S. Tsai, J. M. Godin and Y.-H. Lo, Lab on a Chip (2010).

7. S. H. Cho, C. H. Chen, F. S. Tsai and Y.-H. Lo, Engineering in Medicine and Biology Society, 2009. EMBC 2009. Annual International Conference of the IEEE, 1075 - 1078 (2009).

8. C. Bliss, J. McMullin and C. Backhouse, Lab on a Chip **8** (1), 143-151 (2008).

9. M. Land and D. Nilsson, *Animal eyes*. (Oxford University Press, USA, 2002).

Chapter 5 or portion thereof has been published in *Applied Physics Letters*, Sung Hwan Cho, Wen Qiao, Frank S. Tsai, Kenichi Yamashita, and Yu-Hwa Lo, 97, 093704 (2010).

Chapter 6

Conclusion

Microfluidic, lab-on-a-chip flow cytometers and μFACS offer the numerous benefits of significant reduction in its size and cost, as well as reductions in required sample and reagent volumes, thus lowering the cost of each run and ensuring rapid analysis time. In addition, microfluidic platforms enable the high-level integration of

various functional components such as sample pre-treatment (e.g., cell lysing or staining), fluidic pumping and post-sorted cell culturing in order to create a micro total analysis system on a chip (μTAS). Disposable or at least easily replaceable chips further provide a sterile testing environment, thus reducing significantly the chance of cross-contamination and the potential risks of handling biohazardous samples. Furthermore, a closed, integrated testing platform will provide time and cost savings for researchers and clinicians, ultimately opening new doors for biomedical research. The development of a microfluidic flow cytometer or FACS may be the advance bringing a cytometer to every research lab, expediting discovery and understanding in areas such as cancer research, drug development, and genetics to name a few. Low cost, portable microfluidic flow cytometers could allow for HIV monitoring in resource poor areas of Africa and Asia, helping antiretroviral drugs make their way to patients in need. Low cost microfluidic devices could further help patients in affluent countries to receive faster and consistent test results quickly, and may reduce the amount of blood required to be drawn for testing.

In spite of the numerous advantages, a number of important obstacles need to be addressed in a novel and innovative way in order for microfluidic flow cytometers to rival current benchtop flow cytometers. Microfluidic systems, first of all, should be able to deliver all cells along the microfluidic channel at a uniform velocity regardless of the flow velocity to prevent 'coincident events' at the upstream interrogation zone and 'false-sorting' at the downstream sorting junction. Integrated on-chip optical detection systems must demonstrate their ability to truly rival the sensitivity of benchtop flow

cytometers. In addition, selecting the right material for microfluidic devices and developing mass-fabrication techniques are essential to lowering the cost of the microfluidic flow cytometer. Further, while a miniaturized microfluidic flow cytometry or sorting chip seems addressing many of the issues mentioned here, the size and cost of the whole system must still be reduced significantly. Bulky off-chip components such as the lasers, detectors, pumps, actuators, and electronics can make the final chip-interfacing system considerably larger, in turn making the entire microfluidic system less attractive for practical point-of-care applications or on-the-spot testing.

Many researchers including our research group in UCSD have been working hard in order to resolve those issues, resulting in the novel approaches in each part. Fluid focusing three dimensionally inside microfluidic channel using inertial effects may get rid of the use of additional fluidic pumps and enhance the quality of detection signals, and more importantly can reduce the size of the external fluidic system. Teflon AF coated optofluidic waveguides discussed in Chapter 3 of this thesis can enhance the coupling efficiency of photons to fluorescently tagged biological samples, thus increasing detection sensitivity and permitting multi-spot illumination and detection. The demonstration of fast-response actuators (e.g., PZT actuators) in conjunction with a high-speed, low jitter closed loop control system shows potential for μFACS to greatly exceed the demonstrated throughput of higher than 1,000 cells/sec and to rapidly move into the realm of being competitive with benchtop FACS systems as clearly demonstrated in Chapter 4 of this thesis. Newly demonstrated multi-color detection technology discussed in Chapter 5, known as Color-Space-Time (COST) coding, holds

great promise for compactness since the number of required optical components including dichroic filters and PMTs will no longer scale linearly with the number of detection parameters (e.g. the number of fluorescent colors we want to detect).

Upon satisfying these challenging yet achievable requirements, the field of optofluidics (i.e. microfluidics + optics on chip) holds promise for lab-on-a-chip flow cytometry, offering the development of a low-cost, portable flow cytometer and FACS system on a small chip that can be readily afforded by individual clinics and biomedical research labs. More importantly, such an emerging technology could provide point-of-care diagnosis and analysis in remote areas of Africa and Asia where many people continue to struggle with widespread epidemics, such as Malaria and HIV/AIDS. In short, the development of the compact, low-cost microfluidic flow cytometer system will eventually improve quality of people's life globally; and while the technology is not fully ready yet, great strides to the ultimate goal have been already made towards.

Appendix

Fabrication of aspherical polymer lenses using a tunable liquid-filled mold

In this appendix, I would like to introduce another project that I have been actively involved; Bio-inspired fluidic lens and its application to fabricating PDMS aspherical lens. We demonstrate a tunable molding process to fabricate aspherical polymer lenses that can reduce aberrations and the total length of an optical system.

Radius of curvature and conic constant are shown to be the key parameters to characterize the lens profile. The good agreement between the measured profiles and the simulated profiles allows us to design and fabricate lenses of a wide range of user-specified properties. Compared to the conventional aspherical lens fabrication method using injection molding with a diamond-turned mold, the proposed method may yield savings in time and cost.

A. 1. Introduction

A critical step in verifying the design of an optical system is to fabricate a prototype using lenses of designed surface profiles. The information obtained from the prototype may reveal potential issues not conceived in the original design. In most situations, the bottleneck of prototyping is the acquisition of aspherical lenses. Aspherical lenses, when properly designed, can correct aberrations and reduce the total track length of the optical system significantly.

For prototype fabrication dealing with small lens quantities and with constantly changing designs, today's molding techniques for aspherical lens fabrication can be expensive and time consuming [1, 2]. We modified the method of fluidic lens fabrication [1-5] to fabricate tunable liquid-filled molds of designed aspherical profiles. The liquid-filled tunable molds can be used to form solid lenses of complementary shapes to the molds. By controlling the mechanical properties of the elastic membrane of the mold, one can obtain lenses of different aspherical parameters characterized by their curvature and conic constant [6]. A single tunable mold can be used to generate various aspherical

lenses of different curvature and conic constant. To prove the concept and feasibility of the new process using tunable molds, we have used polydimethylsiloxane (PDMS) liquid-filled molds to form PDMS fixed-focused lenses.

A. 2. Tunable liquid-filled mold

We first machined fluidic channels and chambers on a bottom aluminum block and created an array of 4 mm holes on a top aluminum plate as shown in Figure A. 1.

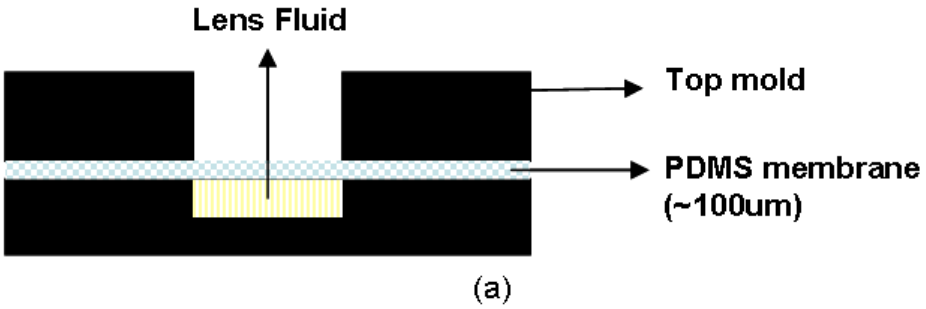

(a)

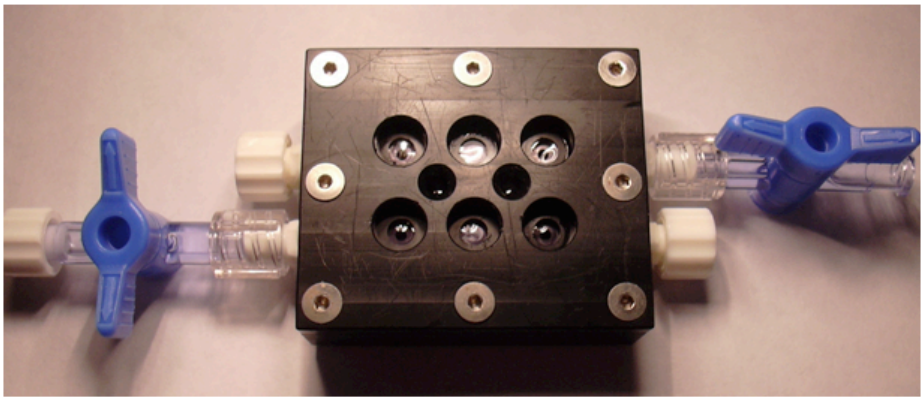

(b)

Figure A.1 (a) Structure of the tunable liquid-filled lens mold. (b) Photograph of the assembled mold that has six liquid-filled lens molds in it. Thin PDMS elastic membrane is sandwiched between the top and the bottom anodized aluminum plates.

To form a thin elastic membrane, we spun PDMS on an optically smooth silicon wafer. The spin-coated PDMS membrane was cured for 2 hours at 65 ^{o}C and peeled off from the wafer. It was then stretched in a controlled amount in a vacuum chamber shown in Figure A.2. Stretching the membrane by a vacuum cup ensures that the stretch on the membrane is rotationally symmetric. Vacuum is slowly applied onto the vacuum cup to stretch the membrane evenly. The slow application of vacuum is very important because when the membrane is quickly stretched, the bubble will be trapped between the membrane and the bottom of the cup.

The amount of prestretch on the membrane is controlled by the height of the cup and is monitored with a handheld pressure gauge. The typical pre-stretch pressure that we have placed into the membrane is around 0.05 ~ 0.08 psi.

Stretching the membrane can avoid wrinkles and produce the required mechanical properties for the designed lens shape. It is critical to uniformly stretch the membrane so that both the stress and the stress gradient of the membrane are radically symmetric. The amount of prestretch is defined as $(\Delta R/R_o) \times 100$ (%), where ΔR is the displacement of the radius by the applied tensile stress and R_o is the initial radius of the elastic membrane before being stretched.

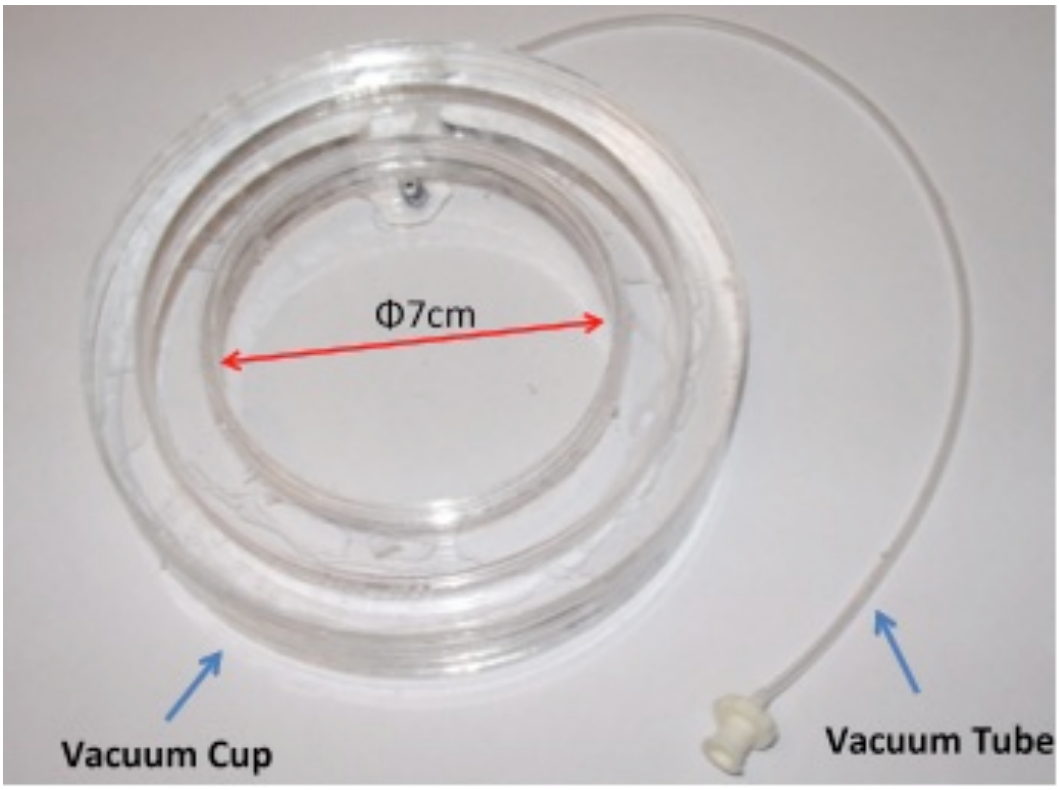

Figure A.2 The customized vacuum cup for evenly stretching elastic membrane radially, ensuring the quality of the membrane.

The prestretched membrane was mounted to the fluidic chambers and sandwiched between the top plate and the bottom block. When the chambers were overfilled with liquid, the mounted PDMS membrane inflated to a convex shape, whereas when under filled the membrane was deflated to a concave shape. The curvature can be controlled by injected fluid volume. Once the desired shape of the liquid-filled mold was achieved, another PDMS prepolymer was poured onto the mold. While being cured, the profile of the liquid-filled mold was transferred onto the cured

lens. The process of casting a fixed-focused plano-convex lens is illustrated in Figure A. 3. The PDMS lens is easily separated from the PDMS membrane of the mold, because they are not chemically cross-linked. The similar process can be applied to fabricate plano-concave PDMS lenses. In addition to the shape of the lens, the thickness of the lens can also be precisely controlled by the amount of poured PDMS. The refractive index of PDMS typically ranges from 1.41 to 1.43 depending on its composition. If lenses of different indices are needed, other polymer materials can be used. Figure A. 4 shows plano-concave and plano-covex PDMS lenses fabricated using the tunable liquid filled mold.

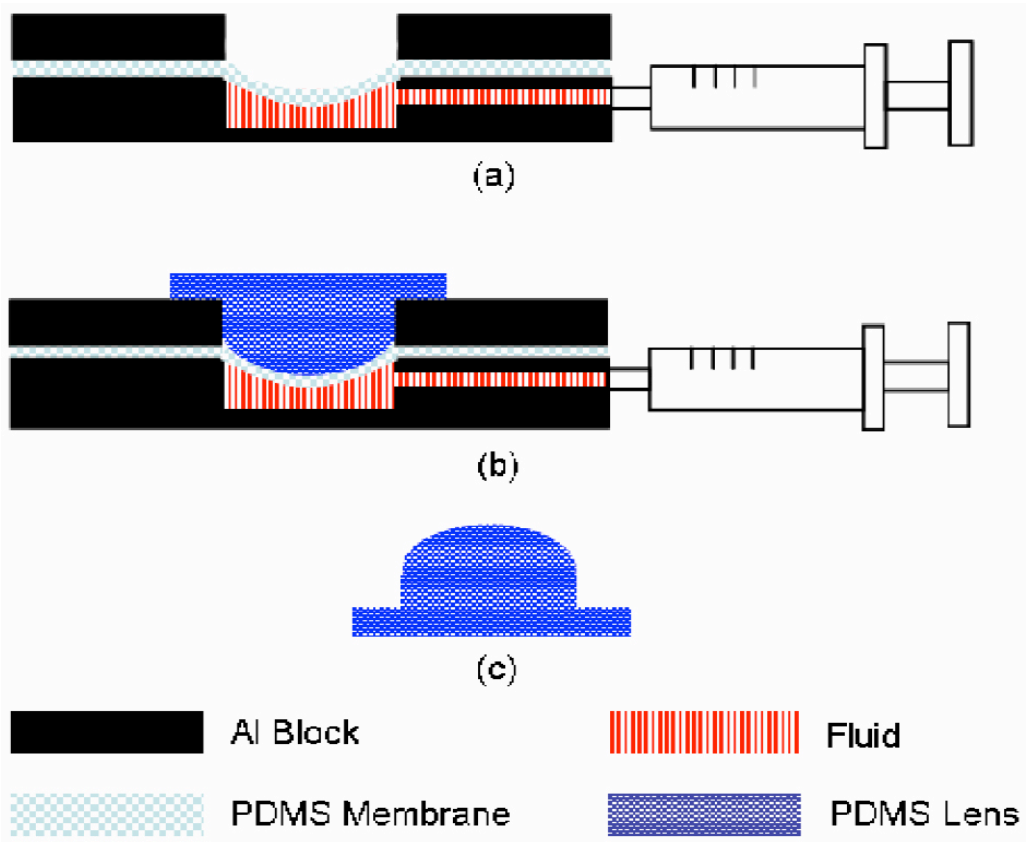

Figure A.3 Process flow of PDMS lens casting: (a) achieve the desired curvature by controlling the fluid volume and/or pressure, (b) pour PDMS prepolymer onto the fluid-filled mold and cure, (c) a plano-convex lens fabricated from liquid filled mold casting.

Figure A.4 (Top) Plano-concave PDMS fixed-focus lens, (Bottom) Plano-convex PDMS lens.

A. 3. Surface roughness measurement

Surface quality of lenses is critical to the device performance. The surface roughness of the lens was measured using an optical interferometer (NT 1100, Veeco). The root-mean-square (RMS) roughness of the lens is less than 6 nm which is adequate for most optical systems except for some highly demanding applications where an RMS roughness of less than 2 nm is required [2]. We suspect the surface roughness may come from the PDMS membrane on the liquid-filled mold and the curing/demolding process. Further investigation is needed to confirm the source(s) of surface roughness and to improve its value.

A. 4. Characterization of aspherical lens profile

After demolding fixed PDMS lenses out of the tunable membrane of the mold structure, the liquid-filled mold is tuned to another shape to create lenses of different lens curvature and profile. By monitoring the shape of the PDMS membrane and adjusting the volume of the fluid, one can obtain the desired curvature of the liquid-filled mold. We characterized the radius curvatures of the tunable membrane using Veeco NT1100 interferometer (Figure A.5). Figure A.6 shows the dependence of the curvature at the center of the liquid-filled mold on the volume of the fluid. The curvature, therefore, can be controlled by the volume of the injected fluid.

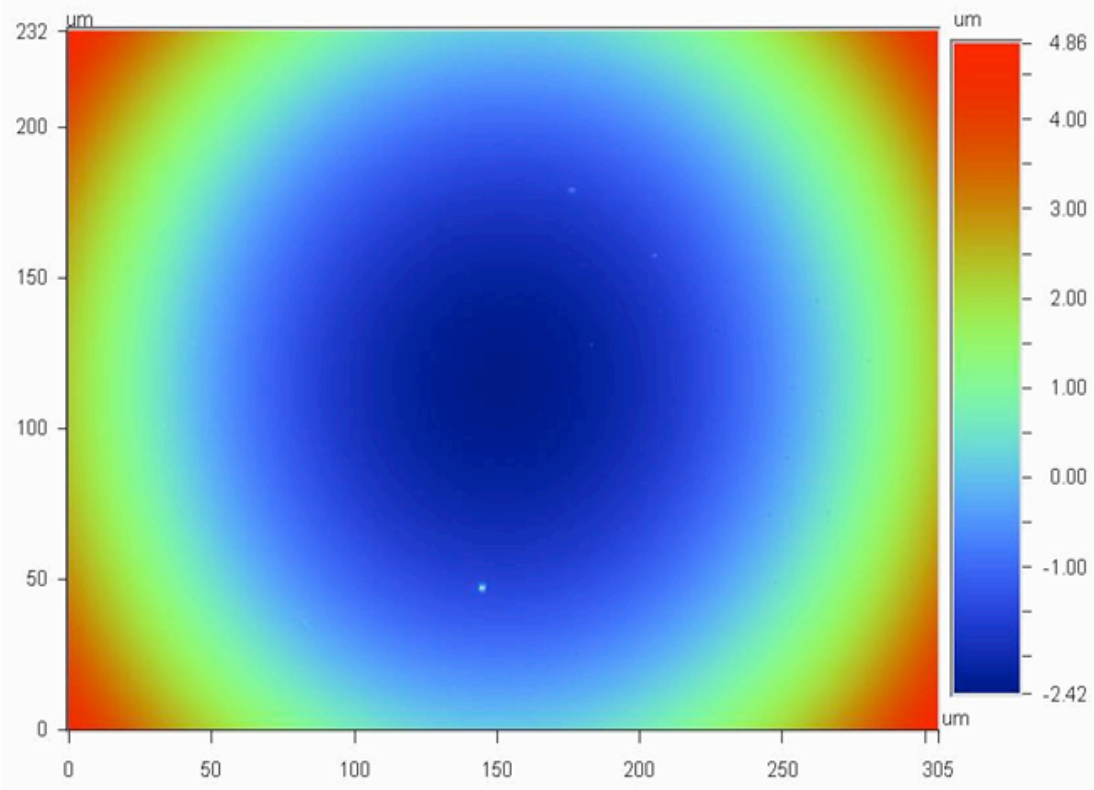

Figure A.5 Surface profile of the PDMS membrane measured by an optical interferometer. It shows rotational symmetry. The root-mean-square (RMS) surface roughness is measured 5.83 nm.

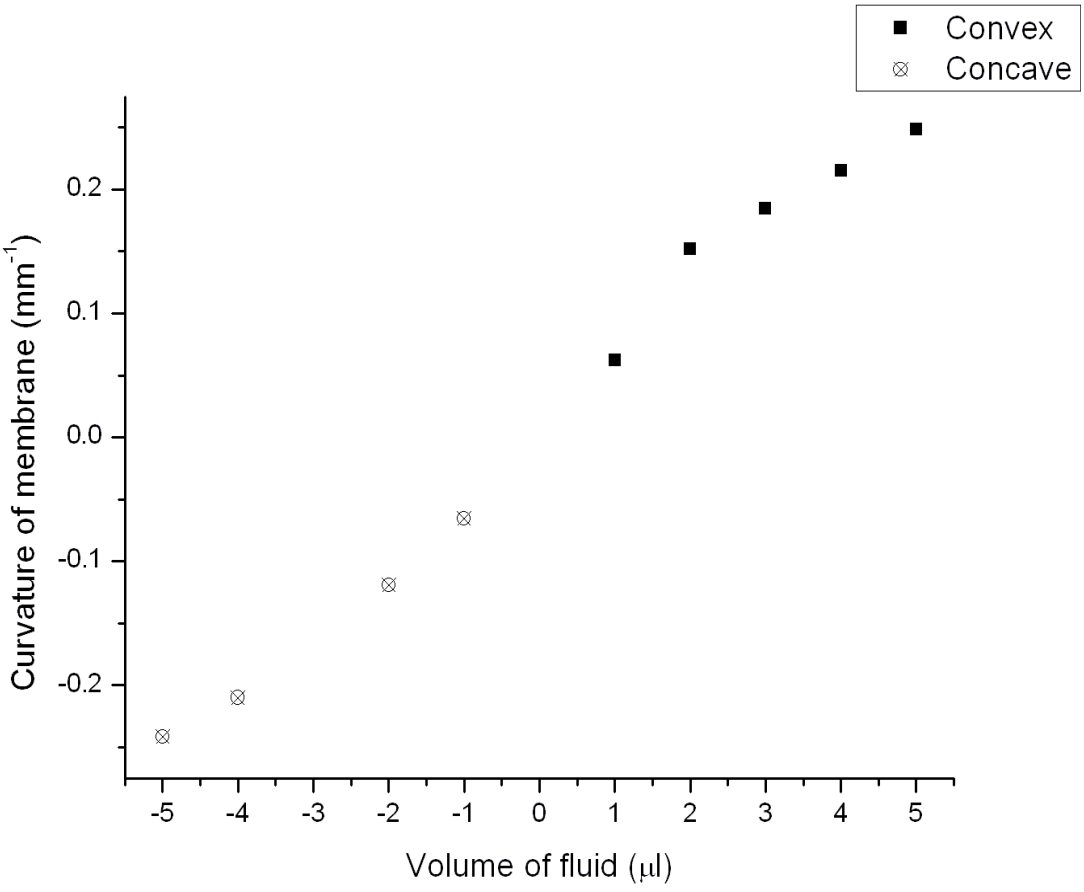

Figure A.6 Dependence of the curvature (mm^{-1}) of the liquid-filled mold on the liquid volume (μl). The curvature of the elastic membrane of the mold can be tuned precisely by the volume of injected fluid.

The lens may have an aspherical profile depending on the mechanical properties of the membrane of the liquid-filled mold. The ability to control the aspherical shape is the most attractive and important feature of this liquid-filled tunable mold technology.

Although higher-order polynomial terms may be added to the elliptical function to better describe the lens profile, most aspherical lenses in practical systems can be optimized using two parameters: curvature and conic constant, in consideration of fabrication tolerance. Therefore, we investigated a large family of aspherical lenses that can be modeled by elliptical functions as in Equation A- (1). The coefficients c and k stand for the curvature at the vertex and the conic constant of the lens, respectively, and r is the radial coordinate perpendicular to the optical axis:

$$z(r) = \frac{cr^2}{1 + \sqrt{1 - (1+k)c^2r^2}} \qquad \text{A - (1)}$$

The lens has a spherical profile if k=0 and a parabolic profile if k=-1. The lens is a hyperboloid if k<-1, and an oblate ellipsoid if k>0 [7]. First-order analysis based on an elastic and infinitely thin membrane under fluidic pressure ahs the shape of a paraboloid (i.e. k=-1) [6]. However, the mechanical properties of most elastomers are nonlinear, and the finite membrane thickness plays an important role.

A. 4. 1. Simulation of the profile of the lens

To more precisely model and predict the profile of the lens, we used finite element analysis software (COMSOL Multiphysics), and the result is shown in Figure A.7. The PDMS membrane was modeled as hyperelastic material according to the Mooney-Rivlin model [8]. The simulated profile of the mold membrane was mathematically fitted to Equation A- (1) using curvature (c) and conic constant (k) as fitting parameters. The curve fitting was performed over 80% of the diameter of the

clear aperture and produced an RMS error of within 30 nm, smaller than one tenth of the wavelength in the visible regime. Image-quality analyses based on ray-tracing simulation using CODE V showed that such deviation in lens profile have insignificant effects, hence demonstrating that Equation A- (1) describes the profiles of molded lenses closely.

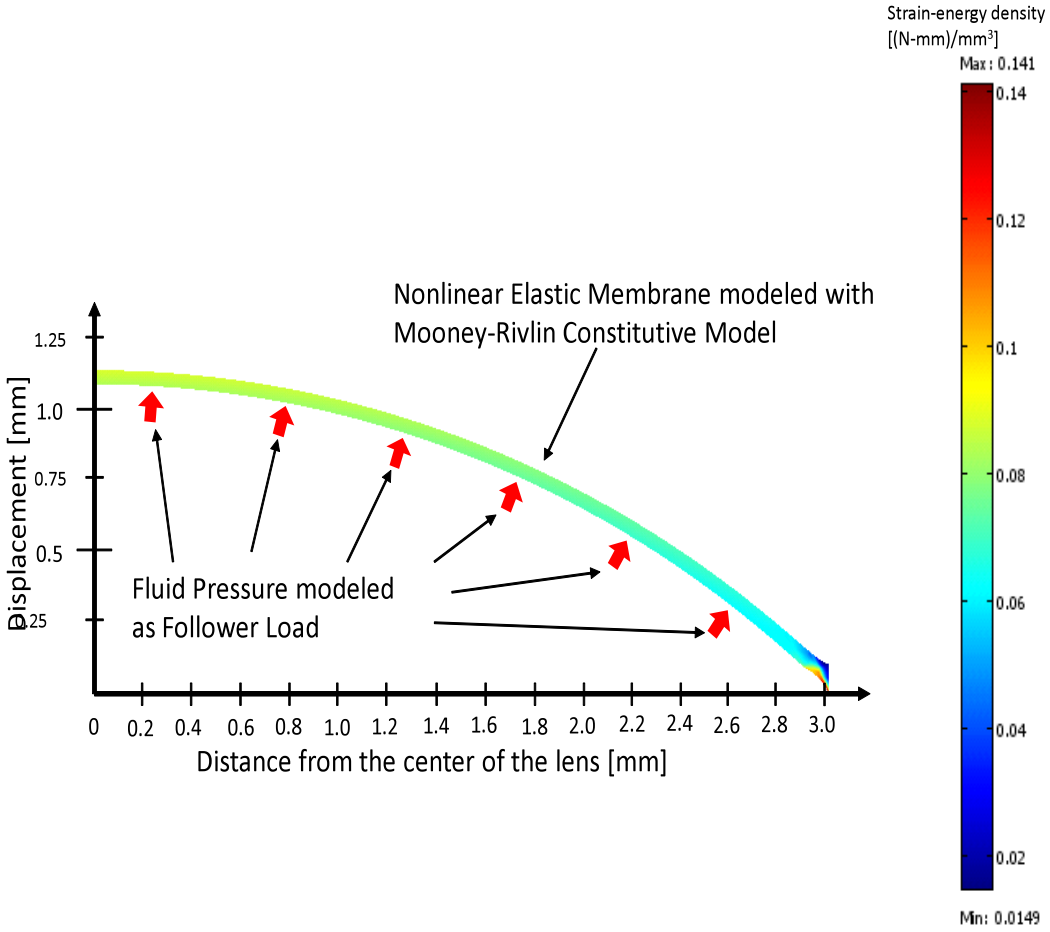

Figure A.7 Example of hyper-elastic modeling of the elastic membrane under fluidic pressure in COMSOL simulation. The fluidic pressure is modeled as follower load and the membrane material property is modeled with Mooney-Rivlin constitutive model.

A. 4. 2. Measurement of the profile of the lens using Shack-Hartmann sensor

An experimental setup using a Shack-Hartmann wavefront sensor (CLAS 2D, WaveFront Science, Inc.) was constructed to measure the profiles of fixed-focused lenses fabricated from a single tunable mold as shown in Figure A. 8 (a)[9]. We measured the wavefront error introduced by the fixed-focused lenses and reconstructed the wavefront from the data of the wavefront sensor. A He-Ne laser beam was expanded by a beam expander and then focused to act as a point source by a microscope objective. The point source was located at a focal distance away from the lens under test. A spherical wavefront out of the point source was supposed to be collimated by the lens-under-test as shown in Figure A.8 (b). The collimation was not perfect owing to lens aberration; however, the collimated wavefront slope was small enough to be measured by the wavefront sensor. The collimated wavefront traveled through one-to-one relay optics to reach the wavefront sensor that measured the real wavefront produced by the lens under test [9]. The relay optics was introduced to alleviate the constraints imposed by the mechanical housing of the wavefront sensor, thus increasing the system's dynamic range for wavefront measurement. The additional wavefront distortion produced by the relay optics has been carefully calibrated not to compromise the accuracy of the measurement. The maximum error in our wavefront measurements, calibrated using precalibrated lenses, was found to be within 76nm. The measured wavefront was fitted to Equation A-(1) and the quality of the fit was examined over 80% of the clear aperture to assure that the RMS fitting errors are within 100 nm (i.e., less than a quarter of the wavelength).

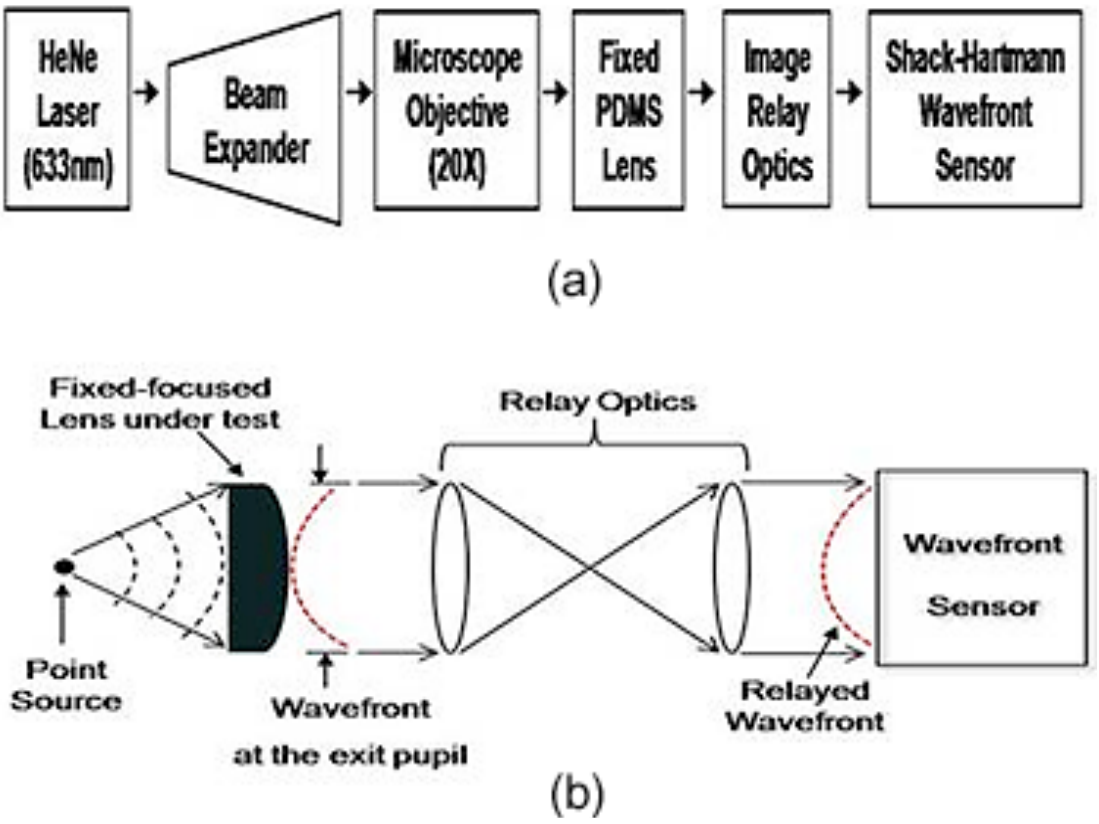

Figure A.8 (a) Measurement setup using a Shack-Hartmann wavefront sensor to measure the lens profile. (b) Distorted wavefront from the lens-under-test is relayed and imaged onto the wavefront sensor. The aspherical profile of the lens is then calculated from the measured wavefront at the exit pupil (red dotted curve)

A. 4. 3. Analysis on the lens profile

Ten PDMS lenses were produced from the same liquid-filled mold tuned to different shapes, and their profiles were measured. The conic constants and radii of

curvature of these lenses were plotted in Figure A.9. The solid curve represents the simulation result obtained from a tunable mold with a 200 μm-thick PDMS membrane and a 10% prestretch.

The good agreement between the measurement and the simulation indicate that one can fabricate aspherical lenses of predictable profiles. The small discrepancy between the simulation and the measurement might be attributed to the weight of PDMS poured onto the mold and the volume shrinkage during curing process[10].

To demonstrate how one can employ the technique of liquid-filled tunable mold to achieve a large variety of aspherical lenses, we show that the membrane thickness and the amount of prestretch can affect the lens profile in a controllable manner. Figure A.10 represents various combinations of curvature and conic constants of a liquid-filled mold having a clear aperture of 3.2 mm in diameter of each PDMS lens.

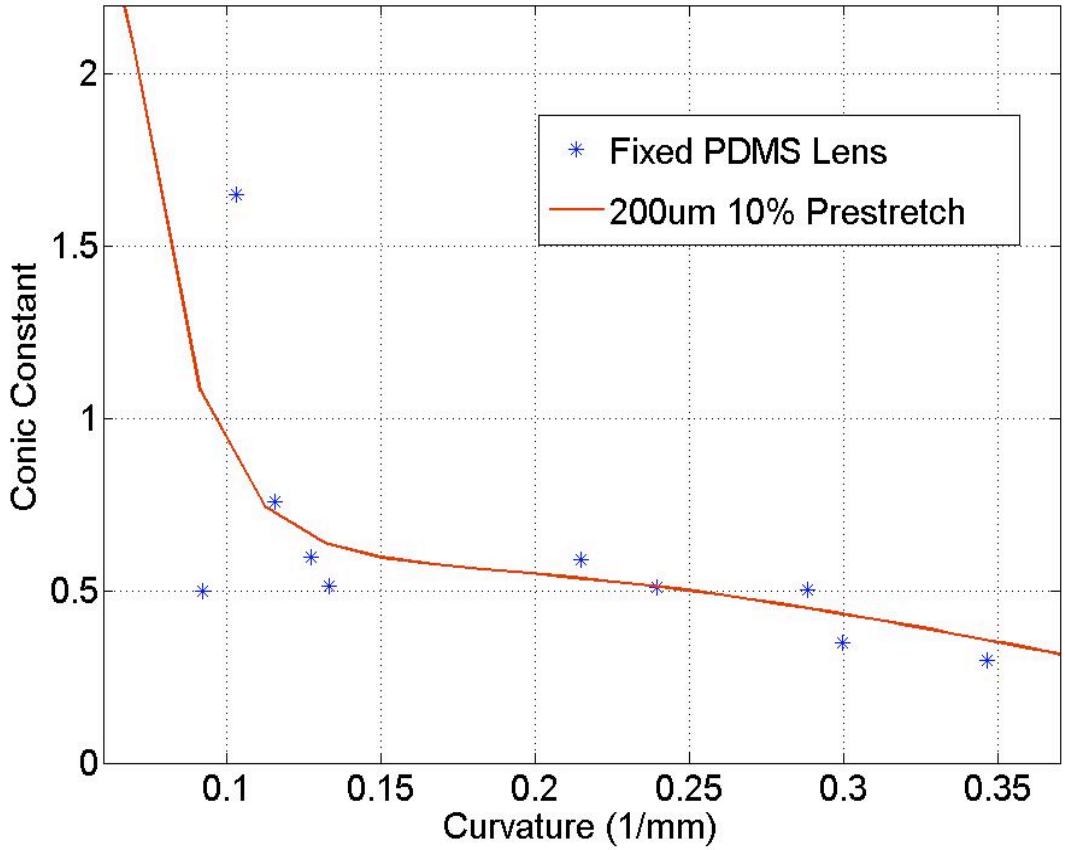

Figure A.9 Measured relationship between the curvature and the conic constants of the fixed-focused lenses (dots). The simulated result (curve) was from a liquid-filled mold with a 200 μm thick PDMS membrane and 10% prestretch.

In Figure A.10, we should point out that the conic constant is of little significance when the lens power is small, as manifested in Equation A –(1) and the CODE V ray-tracing simulations. When the lens power increases, the contribution of conic constant becomes important.

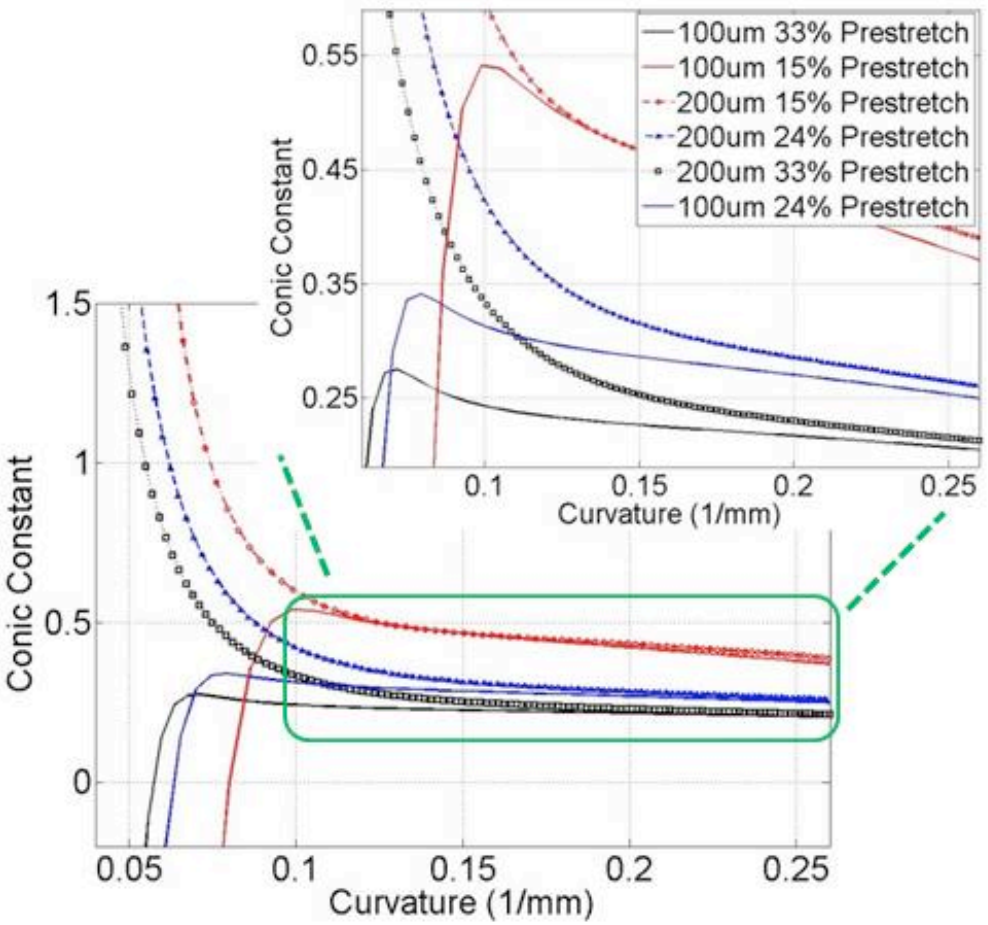

Figure A.10 Curvature versus conic constant of aspherical PDMS fixed-focus lenses. The amount of prestretch and the thickness of the membrane are used as adjustable parameters.

In most cases we studied, positive conic constants were obtained. Working in different parameter space, we anticipate to achieve negative conic constants since the conic constant is equal to -1 for infinitely thin elastic membrane [6]. Besides thickness and prestretch, other design parameters that could affect the lens profiles include the elastic constants and the thickness variation of the membrane in the radial direction.

The key message the authors would like to convey here is that polymer aspherical lenses can be formed using properly engineered liquid-filled molds. This unique capability enables us to construct prototype optical systems in a cost-effective and time efficient manner.

A. 5. Conclusion

In summary, we present a method of liquid-filled tunable mold to fabricate aspherical lenses. The curvature and conic constant of the lens are determined by the amount of fluid in the mold chamber and the membrane characteristics such as elastic properties, thickness, and the percentage of prestretch. The lenses have a surface roughness less than 6 nm. Fitting the aspherical profile of the membrane to the elliptical equation produces an RMS error of less than 30 nm, which justifies the use of radius of curvature and conic constant to describe the profile of aspherical lenses. The simulation results and the experimental data, measured using a Shack-Hartmann wavefront sensor, agree well. More accurate simulations can be obtained by taking into account the effects of gravity and the small volume shrinkage of PDMS while being cured.

References:

1. Y. Aono, M. Negishi and J. Takano, 2000 (unpublished).

2. J. Deegan, W. Hurley, B. Bundschuh and K. Walsh, Precision Glass Molding Technical Brief (Rochester Precision Optics) (2007).

3. F. Tsai, S. Cho, Y. Lo, B. Vasko and J. Vasko, Optics Letters **33** (3), 291-293 (2008).

4. D. Zhang, N. Justis and Y. Lo, Optics Letters **29** (24), 2855-2857 (2004).

5. D. Zhang, N. Justis and Y. Lo, IEEE Journal of selected topics in quantum electronics **11** (1), 97-106 (2005).

6. N. Sugiura and S. Morita, Applied Optics **32** (22), 4181-4186 (1993).

7. R. Fischer and B. Tadic-Galeb, *Optical system design*. (McGraw-Hill Professional, 2000).

8. S. Lee, J. Chan, K. Maung, E. Rezler and N. Sundararajan, Journal of Micromechanics and Microengineering **17**, 843 (2007).

9. R. Rammage, D. Neal and R. Copland, 2002 (unpublished).

10. S. Lee and S. Lee, Microsystem Technologies **14** (2), 205-208 (2008).

Appendix or portion thereof has been published in *Optics Letters*, Sung Hwan Cho, Frank S. Tsai, Wen Qiao, Nam-Hyong Kim, and Yu-Hwa Lo, 34 (5), 605 (2009)